Mathematical Biosciences and Engineering

MBE, 18(5): 5285–5308.
DOI: 10.3934/mbe.2021268
Received: 11 March 2021
Accepted: 25 May 2021
Published: 15 June 2021

http://www.aimspress.com/journal/MBE

Research article

Neuro-Swarm heuristic using interior-point algorithm to solve a third kind of multi-singular nonlinear system

Zulqurnain Sabir[1], Muhammad Asif Zahoor Raja[2], Aldawoud Kamal[3], Juan L.G. Guirao[4,6,*], Dac-Nhuong Le[5], Tareq Saeed[6] and Mohamad Salama[7]

[1] Department of Mathematics and Statistics, Hazara University, Mansehra, Pakistan
[2] Future Technology Research Center, National Yunlin University of Science and Technology, 123 University Road, Section 3, Douliou, Yunlin 64002, Taiwan, China
[3] Department of Mathematics and Statistics, Mutah University Jordan
[4] Department of Applied Mathematics and Statistics, Technical University of Cartagena, Hospital de Marina 30203-Cartagena, Spain
[5] Institute of Research and Development, Duy Tan University, Danang 550000, Vietnam
Faculty of Information Technology, Duy Tan University, Danang 550000, Vietnam
[6] Nonlinear Analysis and Applied Mathematics (NAAM)-Research Group, Department of Mathematics, Faculty of Science, King Abdulaziz University, P.O. Box 80203, Jeddah 21589, Saudi Arabia
[7] Department of Engineering, Applied Science University, Bahrian

* **Correspondence:** Email: juan.garcia@upct.es, jlgarcia@kau.edu.sa.

Abstract: The purpose of the present work is to solve a third kind of multi-singular nonlinear system using the neuro-swarm computing solver based on the artificial neural networks (ANNs) optimized with the effectiveness of particle swarm optimization (PSO) maintained by a local search proficiency of interior-point algorithm (IPA), i.e., ANN-PSO-IPA. An objective function is designed using the continuous mapping of ANN for nonlinear multi-singular third order system of Emden-Fowler equations and optimization of fitness function carried out with the integrated strength of PSO-IPA. The motivation to design the ANN-PSO-IPA is to present a feasible, reliable and feasible framework to handle with such complicated nonlinear multi-singular third order system of Emden-Fowler model. The designed ANN-PSO-IPA is tested for three different nonlinear variants of the multi-singular third kind of Emden-Fowler system. The obtained numerical results on single/multiple executions of the designed ANN-PSO-IPA are used to endorse the precision, viability and reliability.

Keywords: nonlinear singular system; artificial neural networks; multi-singular; interior-point algorithm; statistical analysis; hybrid approach

1. Introduction

The historical Lane-Emden model was introduced first time by astrophysicist Jonathan Homer Lane and Robert Emden [1,2] working on the thermal performance of a spherical cloud of gas and classical law linked to thermodynamics [3]. The singular models have several applications in broad field of applied science and engineering such as catalytic diffusion reactions along with error estimate problems [4], density profile of gaseous star [5], stellar configuration [6], spherical annulus [7], isotropic continuous media [8], the theory of electromagnetic [9] and morphogenesis [10]. It is always not easy to solve the system of singular equations-based models due to their complex nature and singular points. To mention a few schemes that have been applied to solve such models include Legendre wavelets spectral technique [11], Bernoulli collocation scheme [12], variational iteration technique [13], Haar wavelet quasilinearization method [14], spectral collocation scheme [15], differential transformation approach [16] and Adomian decomposition technique [17].

All these above cited approaches have their precise merits and imperfections, however stochastic solver has not been extensively implemented to solve multi-singular third kind of nonlinear system (MS-TKNS) using the artificial neural networks (ANNs) together with particle swarm optimization (PSO) and interior-point algorithm (IPA), i.e., ANN-PSO-IPA. The stochastic computing solvers have been widely applied to resolve numerous applications [18–22]. Recently, the stochastic solvers presented the solution of models for financial market forecasting [23], prey-predator nonlinear system [24], nonlinear singular functional differential model [25,26], SITR nonlinear system [27,28], singular delay differential system [29], nonlinear periodic boundary value problems [30], HIV nonlinear system [31], SIR nonlinear system of dengue fever [32] and alternative approach based on fuzzy-neuro methods to solve linear and nonlinear optimization problems [33,34]. These submissions enhance the worth of the stochastic solvers to authenticate the convergence and precision of the suggested ANN-PSO-IPA. The general form of the MS-TKNS is written as [35]:

$$\begin{cases} \dfrac{d^3U}{d\chi^3}+\dfrac{2\alpha_1}{\chi}\dfrac{d^2U}{d\chi^2}+\dfrac{P(P-1)}{\chi^2}\dfrac{dU}{d\chi}+H_1(\chi)F_1(U,V)=G_1(\chi), \\ \dfrac{d^3V}{d\chi^3}+\dfrac{2\alpha_2}{\chi}\dfrac{d^2V}{d\chi^2}+\dfrac{Q(Q-1)}{\chi^2}\dfrac{dV}{d\chi}+H_2(\chi)F_2(U,V)=G_2(\chi), \\ U(0)=A, \dfrac{dU(0)}{d\chi}=\dfrac{d^2U(0)}{d\chi^2}=0, \\ V(0)=B, \dfrac{dV(0)}{d\chi}=\dfrac{d^2V(0)}{d\chi^2}=0. \end{cases} \tag{1}$$

Where F_1 and F_2 are the nonlinear functions, P and Q are positive constants, G_1 and G_2 are indicated as a source functions.

The purpose of this study is to present the solution of the model (1) via intelligent computing ANN-PSO-IPA. The contributions of the paper are as follows:

- A novel neuro-swarm computing intelligent heuristics ANN-PSO-IPA is accessible for multi-singular nonlinear third order EF-SDEs.
- The overlapping outcomes of the proposed ANN-PSO-IPA with the exact outcomes for three examples of MS-TKNS enhance the exactness, consistency and convergence.
- Authorization of the precise performance is validated via statistical remark using the ANN-PSO-IPA based on Theil's Inequality Coefficient (TIC), Root Mean Square Error (RMSE), Variance Account For (VAF), Semi Interquartile (SI) Range.
- Beside practically precise continuous outcomes on whole input training intermission, an easy implementable process, simplicity in perception, stability and robustness are other well-intentioned announcements for the designed neuro-swarm intelligent computing approach.

The remaining structure of the current study is given as: Section 2 indicates the design methodology through PSO-IPA. The mathematical form of performance measures can be found in section 3. Section 4 shows the numerical results of the designed ANN-PSO-IPA. In the final section, final submissions and future guidance are provided.

2. Methodology

The design of ANN-PSO-IPA for MS-TKNS is presented in two steps, given as:
Step 1: An error based objective function is accessible by using the mean square error sense.
Step 2: The learning procedure of the structures is presented using the hybrid of PSO-IPA.

2.1 ANN modeling

The ANNs are famous to solve the various applications in different domain of applied science and engineering. The proposed outcomes are denoted by $U(\chi)$ and $V(\chi)$, while $\frac{d^nU}{d\chi^n}$ and $\frac{d^nV}{d\chi^n}$ show the n[th] derivative, mathematically given as:

$$\left[\widehat{U}(\chi),\widehat{V}(\chi)\right]=\left[\sum_{i=1}^{m}a_{U,i}Z(w_{U,i}\chi+\phi_{U,i}),\sum_{i=1}^{m}a_{V,i}Z(w_{V,i}\chi+\phi_{V,i})\right],$$
$$\left[\frac{d^n\widehat{U}}{d\chi^n},\frac{d^n\widehat{V}}{d\chi^n}\right]=\left[\sum_{i=1}^{m}a_{U,i}\frac{d^n}{d\chi^n}Z(w_{U,i}\chi+\phi_{U,i}),\sum_{i=1}^{m}a_{V,i}\frac{d^n}{d\chi^n}Z(w_{V,i}\chi+\phi_{V,i})\right]. \quad (2)$$

Where m shows the neurons and n is the derivative order. The unknown weight vectors are $a, w$and ϕ. $W=[W_U,W_V]$, for $W_U=[\alpha_U,w_U,\phi_U]$ and $W_V=[\alpha_V,w_V,\phi_V]$. The components of the weight vector are given as:

$$a_U=[a_{U,1},a_{U,2},a_{U,3},\ldots,a_{U,m}],a_V=[a_{V,1},a_{V,2},a_{V,3},\ldots,a_{V,m}],$$
$$w_U=[w_{U,1},w_{U,2},w_{U,3},\ldots,w_{U,m}],w_V=[w_{V,1},w_{V,2},w_{V,3},\ldots,w_{V,m}],$$
$$\phi_U=[\phi_{U,1},\phi_{U,2},\phi_{U,3},\ldots,\phi_{U,m}],\phi_V=[\phi_{V,1},\phi_{V,2},\phi_{V,3},\ldots,\phi_{V,m}].$$

The log-sigmoid $Z(\chi)=\frac{1}{(1+e^{-\chi})}$ is used as an activation function. The updated form of the system

(2) using the approximate results of $\hat{U}(\chi)$ and $\hat{V}(\chi)$ are written as:

$$[\hat{U}(\chi),\hat{V}(\chi)]=\left[\sum_{i=1}^{m}\frac{a_{U,i}}{1+e^{-(w_{U,i}x+\phi_{U,i})}},\sum_{i=1}^{m}\frac{a_{V,i}}{1+e^{-(w_{V,i}x+\phi_{V,i})}}\right],$$

$$\left[\frac{d\hat{U}}{d\chi},\frac{d\hat{V}}{d\chi}\right]=\left[\sum_{i=1}^{m}\frac{a_{U,i}w_{U,i}e^{-(w_{U,i}x+\phi_{U,i})}}{\left(1+e^{-(w_{U,i}x+\phi_{U,i})}\right)^{2}},\sum_{i=1}^{m}\frac{a_{V,i}w_{V,i}e^{-(w_{V,i}x+\phi_{V,i})}}{\left(1+e^{-(w_{V,i}x+\phi_{V,i})}\right)^{2}}\right],$$

$$\left[\frac{d^2\hat{U}}{d\chi^2},\frac{d^2\hat{V}}{d\chi^2}\right]=\begin{bmatrix}\sum_{i=1}^{m}a_{U,i}w_{U,i}^{2}\left\{\frac{2e^{-2(w_{U,i}x+\phi_{U,i})}}{\left(1+e^{-(w_{U,i}x+\phi_{U,i})}\right)^{3}}-\frac{e^{-(w_{U,i}x+\phi_{U,i})}}{\left(1+e^{-(w_{U,i}x+\phi_{U,i})}\right)^{2}}\right\},\\ \sum_{i=1}^{m}a_{V,i}w_{V,i}^{2}\left\{\frac{2e^{-2(w_{V,i}x+\phi_{V,i})}}{\left(1+e^{-(w_{V,i}x+\phi_{V,i})}\right)^{3}}-\frac{e^{-(w_{V,i}x+\phi_{V,i})}}{\left(1+e^{-(w_{V,i}x+\phi_{V,i})}\right)^{2}}\right\}\end{bmatrix}, \tag{3}$$

$$\left[\frac{d^3\hat{U}}{d\chi^3},\frac{d^3\hat{V}}{d\chi^3}\right]=\begin{bmatrix}\sum_{i=1}^{m}a_{U,i}w_{U,i}^{3}\left\{\frac{6e^{-3(w_{U,i}x+\phi_{U,i})}}{\left(1+e^{-(w_{U,i}x+\phi_{U,i})}\right)^{4}}-\frac{6e^{-2(w_{U,i}x+\phi_{U,i})}}{\left(1+e^{-(w_{U,i}x+\phi_{U,i})}\right)^{3}}+\frac{e^{-(w_{U,i}x+\phi_{U,i})}}{\left(1+e^{-(w_{U,i}x+\phi_{U,i})}\right)^{2}}\right\},\\ \sum_{i=1}^{m}a_{V,i}w_{V,i}^{3}\left\{\frac{6e^{-3(w_{V,i}x+\phi_{V,i})}}{\left(1+e^{-(w_{V,i}x+\phi_{V,i})}\right)^{4}}-\frac{6e^{-2(w_{V,i}x+\phi_{V,i})}}{\left(1+e^{-(w_{V,i}x+\phi_{V,i})}\right)^{3}}+\frac{e^{-(w_{V,i}x+\phi_{V,i})}}{\left(1+e^{-(w_{V,i}x+\phi_{V,i})}\right)^{2}}\right\}\end{bmatrix}$$

The error based objective formulation is written as:

$$E=E_1+E_2+E_3, \tag{4}$$

$$E_1=\frac{1}{N}\sum_{m=1}^{N}\left(\chi_m^2\frac{d^3\hat{U}}{d\chi^3}+2\alpha_1\chi_m\frac{d^2\hat{U}}{d\chi^2}+P(P-1)\frac{d\hat{U}}{d\chi}+\chi_m^2H_1F_1(\hat{U},\hat{V})-\chi_m^2G_1\right)^2, \tag{5}$$

$$E_2=\frac{1}{N}\sum_{m=1}^{N}\left(\chi_m^2\frac{d^3\hat{V}}{d\chi^3}+2\alpha_2\chi_m\frac{d^2\hat{V}}{d\chi^2}+Q(Q-1)\frac{d\hat{V}}{d\chi}+\chi_m^2H_2F_2(\hat{U},\hat{V})-\chi_m^2G_2\right)^2, \tag{6}$$

$$E_3=\frac{1}{6}\left(\left(\hat{U}-A\right)^2+\left(\hat{U}_1^{'}\right)^2+\left(\hat{U}_1^{''}\right)^2+\left(\hat{V}-B\right)^2+\left(\hat{V}^{'}\right)^2+\left(\hat{V}^{''}\right)^2\right) \text{ at } \chi=0. \tag{7}$$

Where $N=\frac{1}{h}, x_m=mh$. The Objective functions E_1 and E_2 are associated with the system of differential equations and E_3 is the corresponding initial conditions.

2.2 Optimization procedure

The optimization is performed to solve the MS-TKNS using the hybrid framework of PSO- IPA.

PSO is an effective research method that has widely used as an alternative optimization of genetic algorithms that were discovered by Kennedy and Eberhart [36]. In the theory of search space, a single candidate result of decision variables in the optimization procedure is called a particle and set of these particle formulated a swarms. For the refinement of optimization variables in standard PSO utilized iterative process of optimizing based on local $P_{LB}^{\rho-1}$ and global $P_{GB}^{\rho-1}$ best position of the particle in

the swarm. The mathematical relations of position $\mathbf{X}_i$ along with the velocity $\boldsymbol{V_i}$ in PSO are given, respectively, as follows:

$$X_i^{\rho} = X_i^{\rho-1} + V_i^{\rho-1}, \tag{8}$$

$$V_i^{\rho} = \omega V_i^{\rho-1} + \eta_1(P_{LB}^{\rho-1} - X_i^{\rho-1})r_1 + \eta_2(P_{GB}^{\rho-1} - X_i^{\rho-1})r_2, \tag{9}$$

where ρrepresent the current flight index, the inertia vector is denoted by ω varying between 0 and 1, η_1 and η_2 indicate the cognitive and social accelerations, respectively, while, r_1 and r_2 are vectors form with pseudo real number between 0 and 1. Further information regrading PSO can be seen in [37], while few recent applications address by PSO include parameter estimation [38], nonlinear electric circuits [39], optimize performance of induction generator [40], optimization of permanent magnets synchronous motor [41] and systems of equations based physical models [42].

The quickly converges performance of PSO is attained by the process of hybridization with the appropriate local search approach by taking the PSO best values as an initial weight. Consequently, in the presented study, an effective local search scheme based on interior-point (IPA) is exploited for rapid fine-tuning of the results by the PSO algorithm. The hybrid of PSO-IPA train the ANNs as well as fundamental parameter setting for both PSO and IPA are tabulated in Table 1. Recently, IPA is used to power flow optimization incorporating security constraints [43], multistage nonlinear nonconvex problems [44], image processing [45] and multi-fractional order doubly singular model [46]. The hybrid of PSO-IPA train the decision variables of ANNs as per procedure and settings tabulated in Table 1.

Table 1. Detailed pseudo code of PSO-IPA to solve the nonlinear third order EF-SDEs.

Start of PSO

Step-1: **Initialization**: Generate the primary swarm randomly and amend the parameters of {PSO} and {optimoptions} routine.

Step-2: Fitness Evaluation: Scrutinize the {fitness value} for each particle in Eq (4).

Step-3: **Ranking**: Rank to each particle of the least standards of the {fitness function}

Step-4: Stopping Standards: Stop, if any of the below form achieved

- Selected flights
- Fitness level

When accomplished the above values, then go to Step-5

Step-5: Renewal: The Eqs (8) and (9) are used for the position and velocity.

Step-6: Improvement: Repeat the above steps 02–06, until the entire flights are attained.

Step-7: Storage: The attained best fitness values is stored and elect as the global best particle.

End of PSO

Start the process of PSO-IPA

Inputs: Use the global best values

Output: $\mathbf{W}_{\text{PSO-IPS}}$ are the PSO-IPA's best values

Initialize: Take {global best values} as a {start point}

Termination: Terminate the process, when {Fitness = $E = 10^{-18}$}, {TolX = 10^{-20}}, {TolCon = TolFun = 10^{-21}}, {MaxFunEvals = 260000} and {Generation = 1500}.

While: [Stop]

Fitness Evaluation: The Eq (4) is used for the fitness value E

Adjustments: Invoke the routine {fmincon} for the IP algorithm to adjust the values of the weight vector.

Store to fitness values using the basic form of the weight vector

Store: $\mathbf{W}_{\text{PSO-IPS}}$ values, final adaptive weight values, function count, fitness, time and generations for the present run.

End of the PSO-IPA

3. Performance indices

The current study is associated to present the statistical measures for solving the MS-TKNS. Therefore, three performances based on Theil's inequality coefficient (TIC) mean absolute deviation (MAD) and Variance Account For (VAF) and their global variables are Global TIC (G.TIC), Global MAD (G.MAD) and Global EVAF (G.EVAF) are applied. The mathematical descriptions of these statistical operators are provided as:

$$[\mathrm{TIC}_U,\mathrm{TIC}_V]=\left[\frac{\sqrt{\frac{1}{n}\sum_{i=1}^{n}\left(U(\chi_i)-\widehat{U}(\chi_i)\right)^2}}{\left(\sqrt{\frac{1}{n}\sum_{i=1}^{n}U^2(\chi_i)}+\sqrt{\frac{1}{n}\sum_{i=1}^{n}\widehat{U}^2(\chi_i)}\right)},\frac{\sqrt{\frac{1}{n}\sum_{i=1}^{n}\left(V(\chi_i)-\widehat{V}(\chi_i)\right)^2}}{\left(\sqrt{\frac{1}{n}\sum_{i=1}^{n}V^2(\chi_i)}+\sqrt{\frac{1}{n}\sum_{i=1}^{n}\widehat{V}^2(\chi_i)}\right)}\right], \tag{10}$$

$$[RMSE_U,RMSE_V]=\left[\sqrt{\frac{1}{n}\sum_{i=1}^{n}\left(U_i-\widehat{U}_i\right)^2},\sqrt{\frac{1}{n}\sum_{i=1}^{n}\left(V_i-\widehat{V}_i\right)^2}\right], \tag{11}$$

$$\begin{cases}[VAF_U,VAF_V]=\left[\left(1-\frac{var\left(U(\chi_i)-\widehat{U}(\chi_i)\right)}{var(U(\chi_i))}\right)*100,\left(1-\frac{var\left(V(\chi_i)-\widehat{V}(\chi_i)\right)}{var(V(\chi_i))}\right)*100\right]\\ [EVAF_U,EVAF_V]=[|100-VAF_U|,|100-VAF_V|].\end{cases} \tag{12}$$

4. Results and discussion

In this section, the detail discussion to solve three variants of the MS-TKNS is presented.

Problem 1: Consider the MS-TKNS is:

$$\begin{cases} \dfrac{d^3U}{d\chi^3}+\dfrac{2}{\chi}\dfrac{d^2U}{d\chi^2}+\dfrac{3}{\chi}\dfrac{dU}{d\chi}-U^2V=17e^{\chi^3}+9\chi e^{\chi^3}+72\chi^3e^{\chi^3}+27\chi^6e^{\chi^3}, \\ \dfrac{d^3V}{d\chi^3}+\dfrac{2}{\chi}\dfrac{d^2V}{d\chi^2}+\dfrac{3}{\chi}\dfrac{dV}{d\chi}-UV^2=-19e^{\chi^3}+9\chi e^{-\chi^3}+72\chi^3e^{-\chi^3}-27\chi^6e^{-\chi^3}, \\ U(0)=1,\ \dfrac{dU(0)}{d\chi}=\dfrac{d^2U(0)}{d\chi^2}=0, \\ V(0)=1,\ \dfrac{dV(0)}{d\chi}=\dfrac{d^2V(0)}{d\chi^2}=0. \end{cases} \tag{13}$$

The exact/true solutions of the above Eq (13) are $[e^{\chi^3}, e^{-\chi^3}]$ and the fitness function becomes as:

$$E=\frac{1}{N}\sum_{m=0}^{N}\left(\begin{array}{l}\left(\chi_m\dfrac{d^3\hat{U}}{d\chi^3}+2\dfrac{d^2\hat{U}}{d\chi^2}+3\dfrac{d\hat{U}}{d\chi}-\chi_m\hat{U}^2\hat{V}-\chi_mG_1\right)^2+\\ \left(\chi_m\dfrac{d^3\hat{V}}{d\chi^3}+2\dfrac{d^2\hat{V}}{d\chi^2}+3\dfrac{d\hat{V}}{d\chi}-\chi_m\hat{U}\hat{V}^2-\chi_mG_2\right)^2\end{array}\right) \tag{14}$$
$$+\frac{1}{6}\left(\begin{array}{l}\left(\hat{U}-1\right)^2+\left(\dfrac{d\hat{U}}{d\chi}\right)^2+\left(\dfrac{d^2\hat{U}}{d\chi^2}\right)^2\\ +\left(\hat{V}-1\right)^2+\left(\dfrac{d\hat{V}}{d\chi}\right)^2+\left(\dfrac{d^2\hat{V}}{d\chi^2}\right)^2\end{array}\right).$$

Problem 2: Consider the MS-TKNS is:

$$\begin{cases} \dfrac{d^3U}{d\chi^3}+\dfrac{2}{\chi}\dfrac{d^2U}{d\chi^2}+\dfrac{3}{\chi}\dfrac{dU}{d\chi}+UV^3=4+e^{-3\chi^3}+4e^{-2\chi^3}+6e^{-\chi^3}+19e^{\chi^3}+9\chi e^{\chi^3} \\ \qquad\qquad +72\chi^3e^{\chi^3}+27\chi^6e^{\chi^3}, \\ \dfrac{d^3V}{d\chi^3}+\dfrac{2}{\chi}\dfrac{d^2V}{d\chi^2}+\dfrac{3}{\chi}\dfrac{dV}{d\chi}+U^3V=4-17e^{-\chi^3}+4e^{2\chi^3}+6e^{\chi^3}+3e^{3\chi^3}-9\chi e^{-\chi^3} \\ \qquad\qquad +72\chi^3e^{-\chi^3}-27\chi^6e^{-\chi^3}, \\ U(0)=2,\dfrac{dU(0)}{d\chi}=\dfrac{d^2U(0)}{d\chi^2}=0, \\ V(0)=2,\dfrac{dV(0)}{d\chi}=\dfrac{d^2V(0)}{d\chi^2}=0. \end{cases} \tag{15}$$

The true solutions of the above equation are $[1+e^{\chi^3}, 1+e^{-\chi^3}]$ and the objective function becomes as:

$$E=\frac{1}{N}\sum_{m=0}^{N}\left(\begin{array}{l}\left(\chi_m\dfrac{d^3\hat{U}}{d\chi^3}+2\dfrac{d^2\hat{U}}{d\chi^2}+3\dfrac{d\hat{U}}{d\chi}+\chi_m\hat{U}\hat{V}^3-\chi_mG_1\right)^2+\\ \left(\chi_m\dfrac{d^3\hat{V}}{d\chi^3}+2\dfrac{d^2\hat{V}}{d\chi^2}+3\dfrac{d\hat{V}}{d\chi}+\chi_m\hat{U}^3\hat{V}-\chi_mG_2\right)^2\end{array}\right)+\frac{1}{6}\left(\begin{array}{l}\left(\hat{U}-2\right)^2+\left(\dfrac{d\hat{U}}{d\chi}\right)^2+\left(\dfrac{d^2\hat{U}}{d\chi^2}\right)^2\\ +\left(\hat{V}-2\right)^2+\left(\dfrac{d\hat{V}}{d\chi}\right)^2+\left(\dfrac{d^2\hat{V}}{d\chi^2}\right)^2\end{array}\right). \tag{16}$$

Problem 3: Consider the MS-TKNS is:

$$\begin{cases} \frac{d^3U}{d\chi^3}+\frac{6}{\chi}\frac{d^2U}{d\chi^2}-\frac{2}{\chi}\frac{dU}{d\chi}+(1-U)V=42-6\chi-\chi^3+\chi^6, \\ \frac{d^3V}{d\chi^3}+\frac{6}{\chi}\frac{d^2V}{d\chi^2}-\frac{2}{\chi}\frac{dV}{d\chi}-U(1-V)=-42+6\chi-\chi^3-\chi^6, \\ U(0)=1,\frac{dU(0)}{d\chi}=\frac{d^2U(0)}{d\chi^2}=0, \\ V(0)=1,\frac{dV(0)}{d\chi}=\frac{d^2V(0)}{d\chi^2}=0. \end{cases} \tag{17}$$

The true solutions of the Eq (17) are $[1+\chi^3, 1-\chi^3]$ and the fitness function becomes as:

$$E=\frac{1}{N}\sum_{m=0}^{N}\left(\begin{pmatrix}\left(\chi_m\frac{d^3\widehat{U}}{d\chi^3}+6\frac{d^2\widehat{U}}{d\chi^2}-2\frac{d\widehat{U}}{d\chi}+\chi_m(1-\widehat{U})\widehat{V}-\chi_m G_1\right)^2+\\ \left(\chi_m\frac{d^3\widehat{V}}{d\chi^3}+6\frac{d^2\widehat{V}}{d\chi^2}-2\frac{d\widehat{V}}{d\chi}+\chi_m\widehat{U}(1-\widehat{V})-\chi_m G_2\right)^2\end{pmatrix}\right. \\ \left.+\frac{1}{6}\begin{pmatrix}\left(\widehat{U}-1\right)^2+\left(\frac{d\widehat{U}}{d\chi}\right)^2+\left(\frac{d^2\widehat{U}}{d\chi^2}\right)^2\\ +\left(\widehat{V}-1\right)^2+\left(\frac{d\widehat{V}}{d\chi}\right)^2+\left(\frac{d^2\widehat{V}}{d\chi^2}\right)^2\end{pmatrix}\right). \tag{18}$$

In order to find the proposed solutions of the Problems 1, 2 and 3 based on the MS-TKNS by using the proposed solver ANN-PSO-IPA for 40 multiple trials to achieve the adaptable parameters. The plots of the weight sets are shown in Figure 1 for $U(\chi)$ and $V(\chi)$, respectively. These weights are the decision variables of ANNs as presented in equations 3 such that the fitness functions in (14), (16) and (18) for respective problems 1, 2 and 3 are optimized with PSO-IPA, i.e., initially for global search efficacy of PSO and fine tune with IPA for rapid local search. These sets of weights are applied in first equation of set (3) to find approximate solutions to the three problems and the mathematical form are given as:

$$\widehat{U}_{P-1}=\frac{-6.786}{1+e^{-(-11.644\chi+15.35)}}+\frac{4.539}{1+e^{-(-1.651\chi+2.200)}} +\frac{-0.558}{1+e^{-(-8.143\chi+9.243)}}+\ldots+\frac{4.377}{1+e^{-(0.019\chi+2.086)}}, \tag{19}$$

$$\widehat{U}_{P-2}=\frac{1.008}{1+e^{-(1.230\chi+0.015)}}+\frac{4.209}{1+e^{-(12.45\chi-15.681)}} +\frac{0.336}{1+e^{-(-6.716\chi+6.309)}}+\ldots-\frac{0.329}{1+e^{-(-1.124\chi+3.324)}}, \tag{20}$$

$$\widehat{U}_{P-3}=\frac{-0.017}{1+e^{-(4.530\chi-3.801)}}+\frac{4.682}{1+e^{-(2.529\chi+2.999)}} +\frac{5.098}{1+e^{-(0.715\chi+0.913)}}+\ldots+\frac{3.159}{1+e^{-(-2.099\chi+8.587)}}, \tag{21}$$

$$\hat{V}_{P-1} = \frac{5.049}{1+e^{-(-2.457\chi+2.070)}} + \frac{0.068}{1+e^{-(0.380\chi+1.115)}} + \frac{-0.041}{1+e^{-(-0.464\chi+0.215)}} + \ldots + \frac{1.790}{1+e^{-(2.540\chi-1.143)}}, \tag{22}$$

$$\hat{V}_{P-2} = \frac{-1.550}{1+e^{-(0.418\chi-1.586)}} - \frac{0.692}{1+e^{-(4.495\chi+2.403)}} + \frac{1.550}{1+e^{-(-3.258\chi+2.387)}} + \ldots - \frac{0.253}{1+e^{-(-0.32\chi-0.418)}}, \tag{23}$$

$$\hat{V}_{P-3} = \frac{2.237}{1+e^{-(0.454\chi-0.035)}} - \frac{0.825}{1+e^{-(1.564\chi+0.541)}} - \frac{0.249}{1+e^{-(1.204\chi-0.301)}} + \ldots - \frac{0.771}{1+e^{-(-1,792\chi+0.440)}}, \tag{24}$$

The optimization of the MS-TKNS is performed for the problems 1, 2 and 3 using the proposed solver ANN-PSO-IPA for 40 independent trials. Set of weights and results comparison are plotted graphically in Figure 1. It is specified that the exact and proposed solutions overlapped for both the indexes $\hat{U}(\chi)$ and $\hat{V}(\chi)$ of the problems 1, 2 and 3. This exact matches of the outcomes shows the correctness of the proposed methodology ANN-PSO-IPA. In order to calculate the comparison of the numerical results, the plots of the absolute error (AE) are drawn in Figure 2(a),(b) for $\hat{U}(\chi)$ and $\hat{V}(\chi)$. One can observe that most of the AE values of problems 1–3 for $\hat{U}(\chi)$ lie in the range of 10^{-6} to 10^{-7}, 10^{-4} to 10^{-6} and 10^{-6} to 10^{-8}, while, for $\hat{V}(\chi)$, these values lie around 10^{-5} to 10^{-6}, 10^{-3} to 10^{-4} and 10^{-6} to 10^{-7}. The plots of the performance measures through fitness, RMSE, TIC and EVAF are drawn in the Figure 2(c),(d) for $\hat{U}(\chi)$ and $\hat{V}(\chi)$. It is seen that the fitness values lie around to 10^{-06} to 10^{-08}, for problems 1 and 3, while the fitness values for Problem 2 are close to 10^{-08}. The RMSE values of $\hat{U}(\chi)$ and $\hat{V}(\chi)$ for problem 1 and 3 are close to 10^{-6} to 10^{-8}, while for Problem 2, the RMSE lie 10^{-4}–10^{-6} for $\hat{U}(\chi)$ and 10^{-2}–10^{-4} for $\hat{V}(\chi)$. The TIC performance lie around 10^{-6}–10^{-8} for both indexes of all the Problems. The EVAF values for problem 1 and 3 lie 10^{-10}–10^{-12} for both the indexes, while it lies around 10^{-8}–10^{-10} for problem 2.

The convergence measures for the Problems 1–3 based on the MS-TKNS using the Fitness, histograms and boxplots for 10 numbers of neurons are provided in Figure 3. It is shown that most of the fitness values lie around 10^{-4}–10^{-6} for Problem 1 and 3, while for Problem 3 these values lie around 10^{-6}–10^{-8}. The convergence of both the indexes of all the problems for RMSE, TIC and EVAF is provided in Figures 4–9. Most of the values for both the indexes of all the problems lie in good ranges.

For more accuracy and precision, statistical indices are performed based on minimum (Min), standard deviation (SD), mean, SI range and Median. SI Range is one half of the difference of Q_3 = 75% data, i.e., 3rd quartile and Q_1 = 25% data, i.e., 1st quartile is calculated for 40 trials of ANN-PSO-IPA to solve three different problems of MS-TKNS. These statistical based outcomes for Problems 1–3 are tabulated in Tables 2 and 3 for the indexes $\hat{U}(\chi)$ and $\hat{V}(\chi)$. It is observed that most of the $\hat{U}(\chi)$ and $\hat{V}(\chi)$ values for Problems 1–3 lie in the best ranges. The global performance G.FIT, G.RMSE, G.TIC and G.EVAF of $\hat{U}(\chi)$ and $\hat{V}(\chi)$ for Problems 1, 2 and 3 are tabulated in Table 4. These performances of the global values for Problems 1, 2 and 3 for 40 independent trials are provided. The magnitude (Mag) and Median values for all Problems using the indexes $\hat{U}(\chi)$ and $\hat{V}(\chi)$ proved very good results based on the statistical global operators.

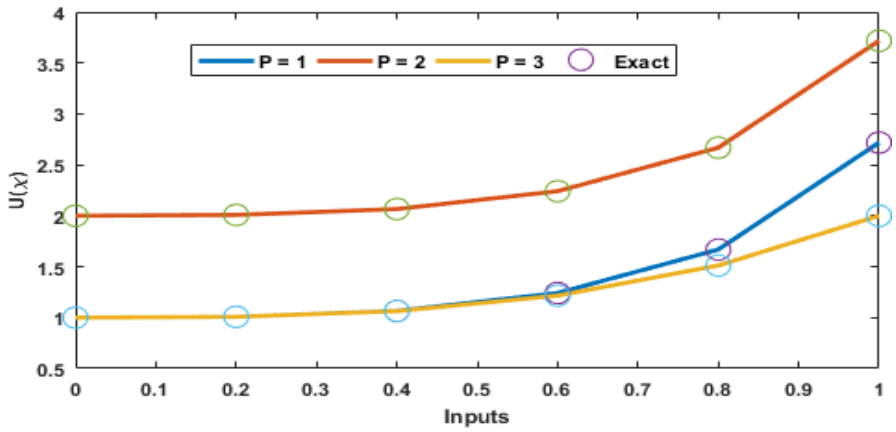

(a) Results of $\hat{U}(\chi)$ for Problems 1, 2 and 3.

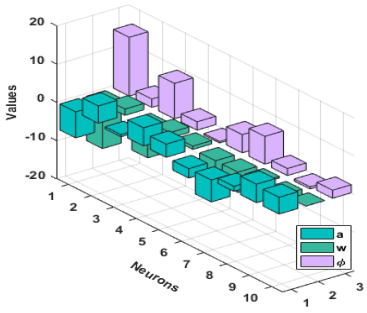

(b) Weights of Problem 1 for $\hat{U}(\chi)$.

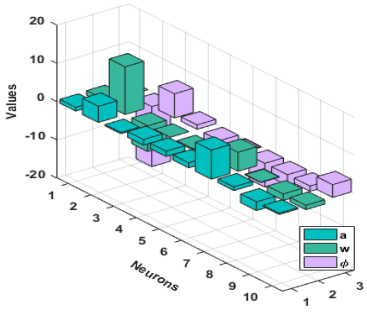

(c) Weights of Problem 2 for $\hat{U}(\chi)$.

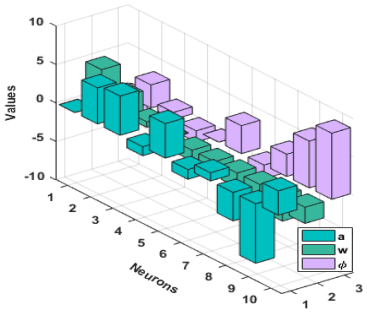

(d) Weights of Problem 3 for $\hat{U}(\chi)$.

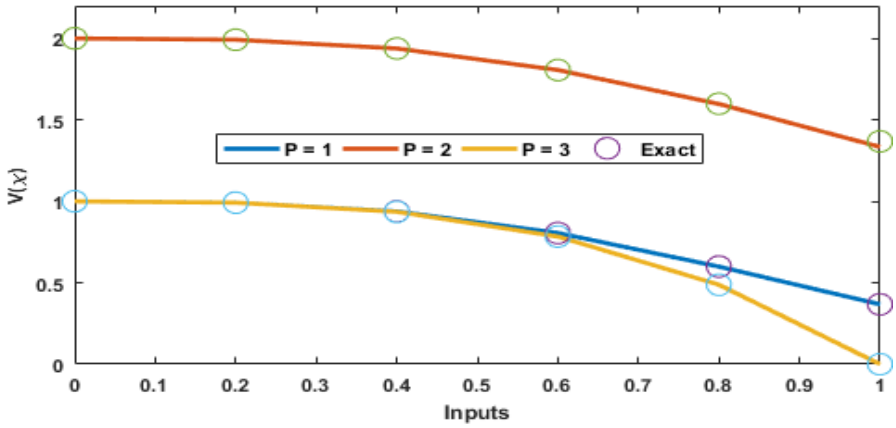

(e) Results of $\hat{V}(\chi)$ for Problems 1, 2 and 3.

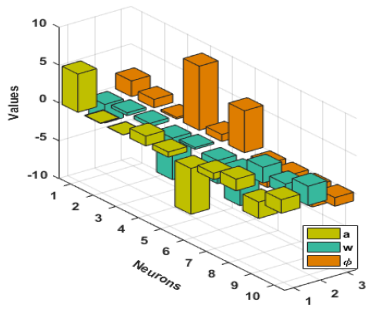

(f) Weights of Problem 1 for $\hat{V}(\chi)$.

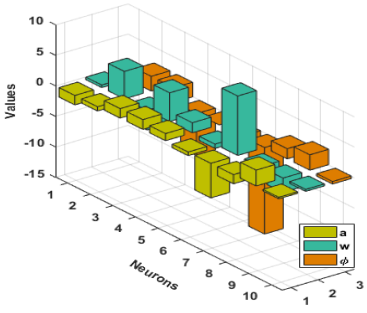

(g) Weights of Problem 2 for $\hat{V}(\chi)$.

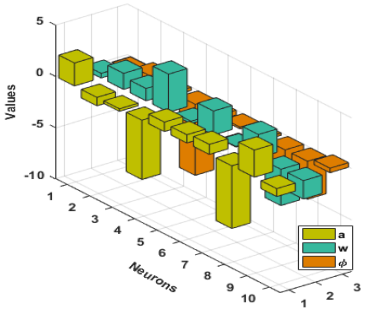

(h) Weights of Problem 3 for $\hat{V}(\chi)$.

Figure 1. Best weight sets and result comparisons for Problems 1, 2 and 3.

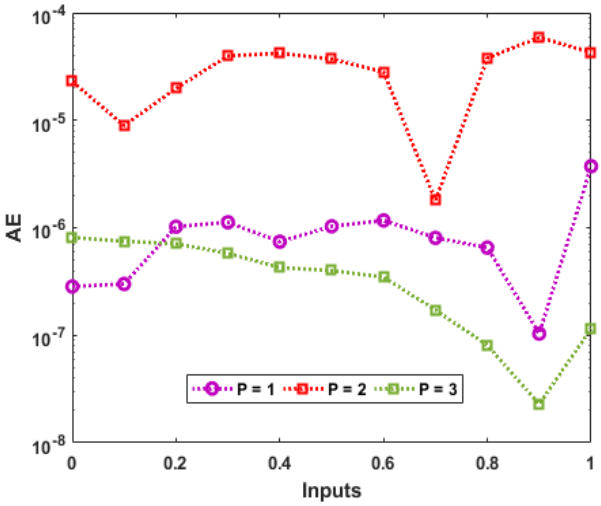

(a) AE of Problems 1, 2 and 3 for $\hat{U}(\chi)$.

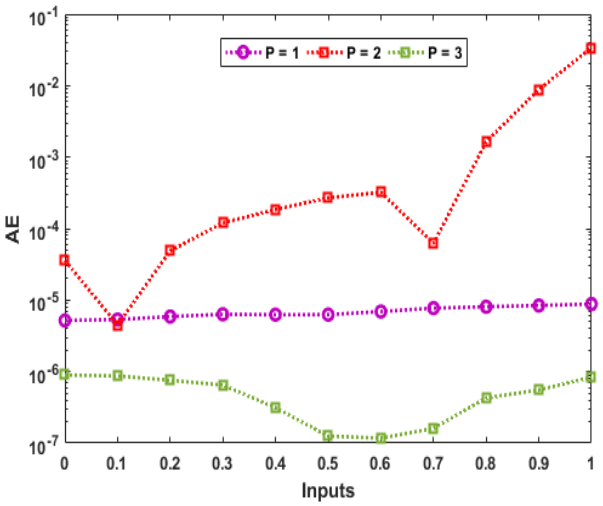

(b) AE of Problems 1, 2 and 3 for $\hat{V}(\chi)$.

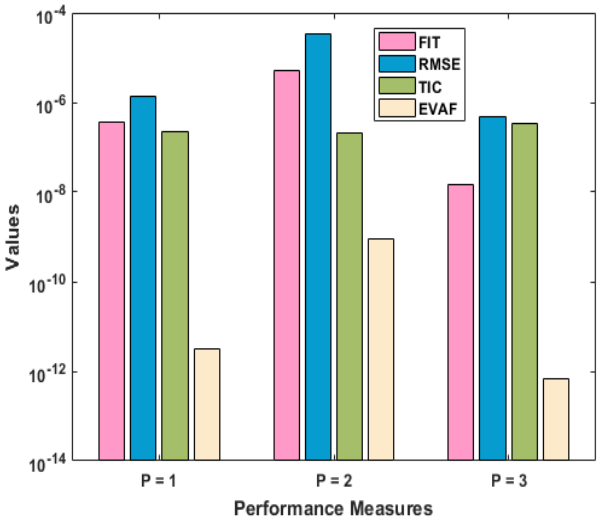

(c) Performance measures of Problem 1, 2 and 3 for $\hat{U}(\chi)$.

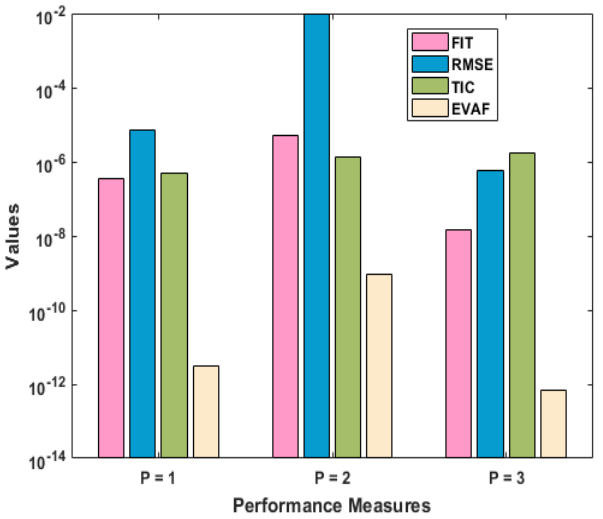

(d) Performance measures of Problem 1, 2 and 3 for $\hat{V}(\chi)$.

Figure 2. Absolute error and performance indices for Problems 1, 2 and 3.

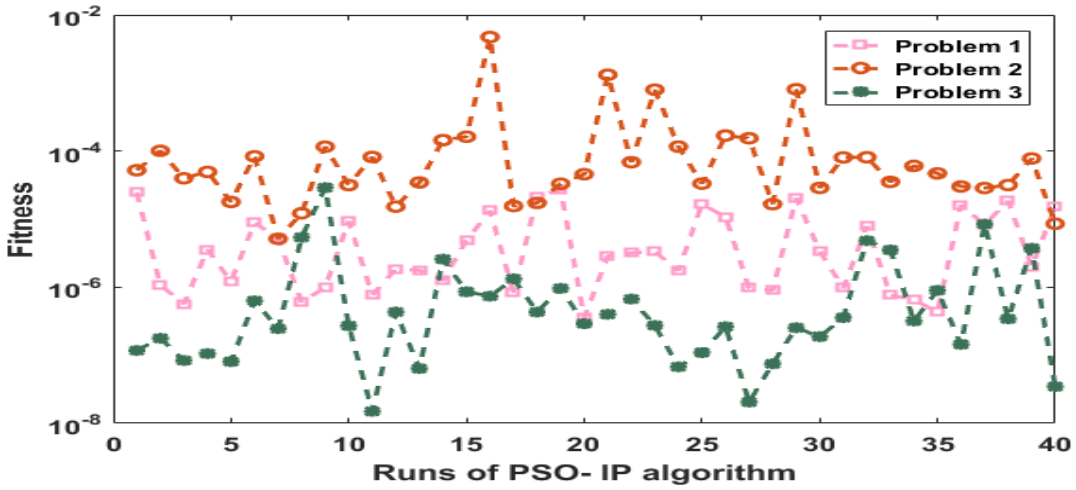

Convergence indices for all problems of the MS-TKNS for the Fitness values.

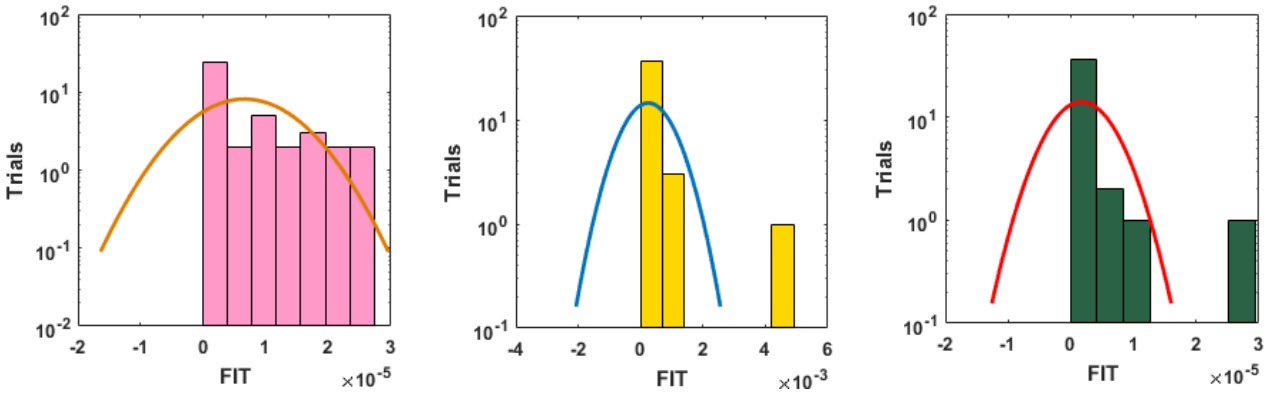

(a) Histogram: Problem-1. (b) Histogram: Problem 2. (c) Histogram: Problem 3.

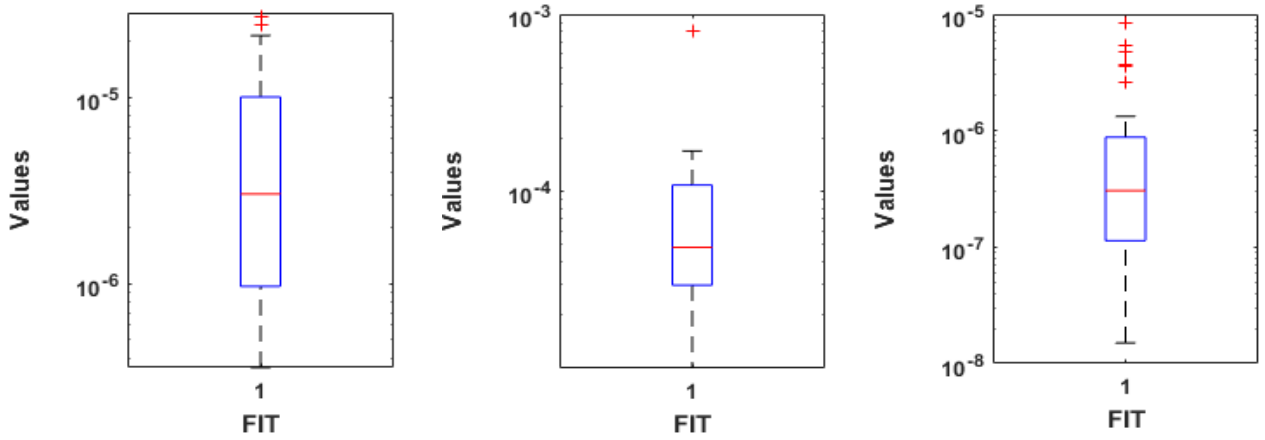

(d) Boxplots: Problem 1. (e) Boxplots: Problem 2. (f) Boxplots: Problem 3.

Figure 3. Convergence procedures for the Problems 1, 2 and 3 based on the MS-TKNS using the Fitness, histograms and boxplots for 10 neurons.

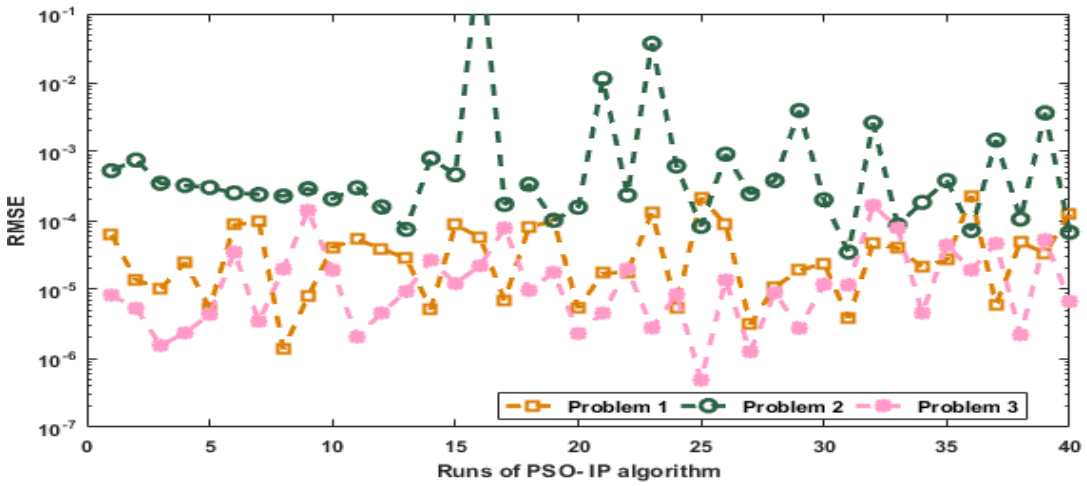

Convergence indices of $\hat{U}(\chi)$ for each problem of the MS-TKNS for the RMSE values.

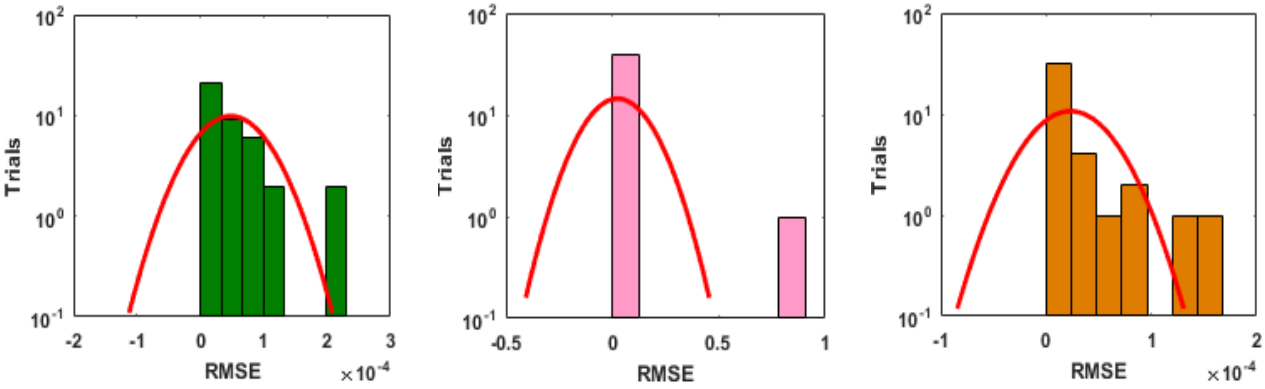

(a): Histogram: Problem-1. (b): Histogram: Problem 2. (c): Histogram: Problem 3.

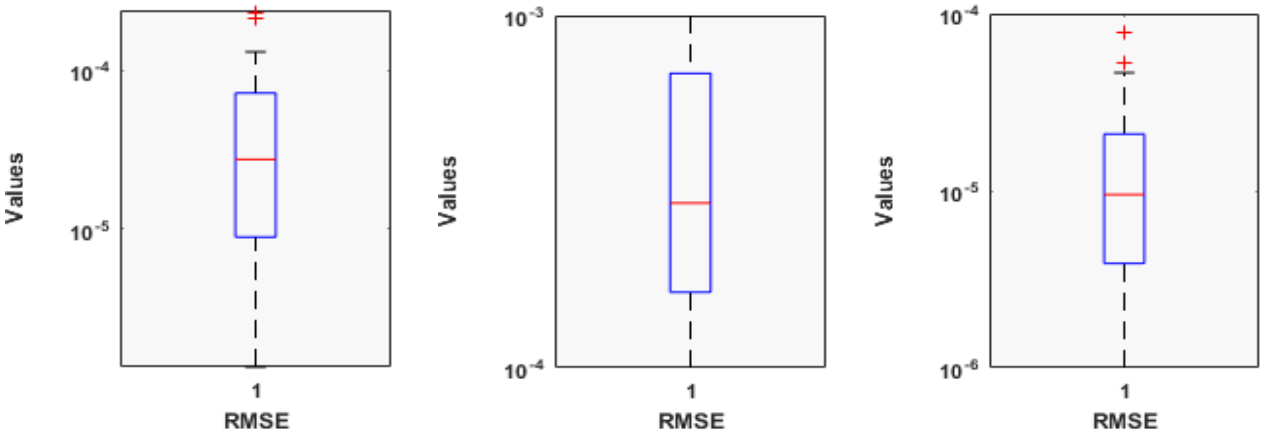

(d): Boxplot: Problem 1. (e): Boxplot: Problem 2. (f): Boxplot: Problem 3.

Figure 4. Convergence investigations of $\hat{U}(\chi)$ for the Problems 1, 2 and 3 based on the MS-TKNS using the Fitness, histograms and boxplots for 10 neurons.

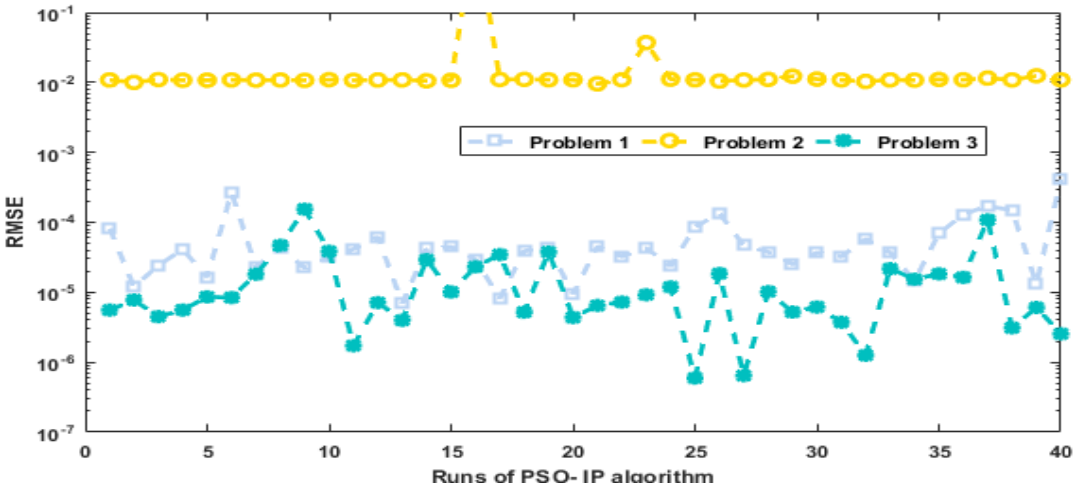

Convergence indices of $\hat{V}(\chi)$ for each problem of the MS-TKNS for the RMSE values.

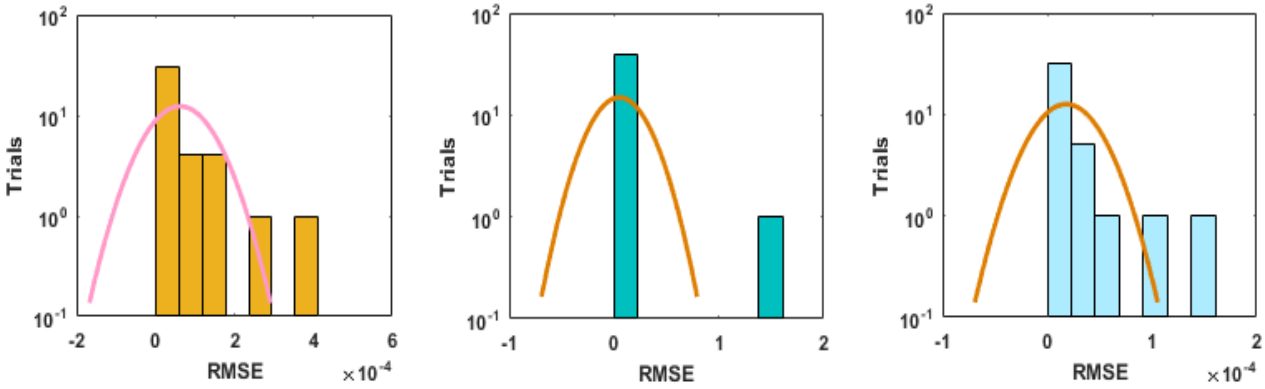

(a) Histogram: Problem-1. (b) Histogram: Problem 2. (c) Histogram: Problem 3.

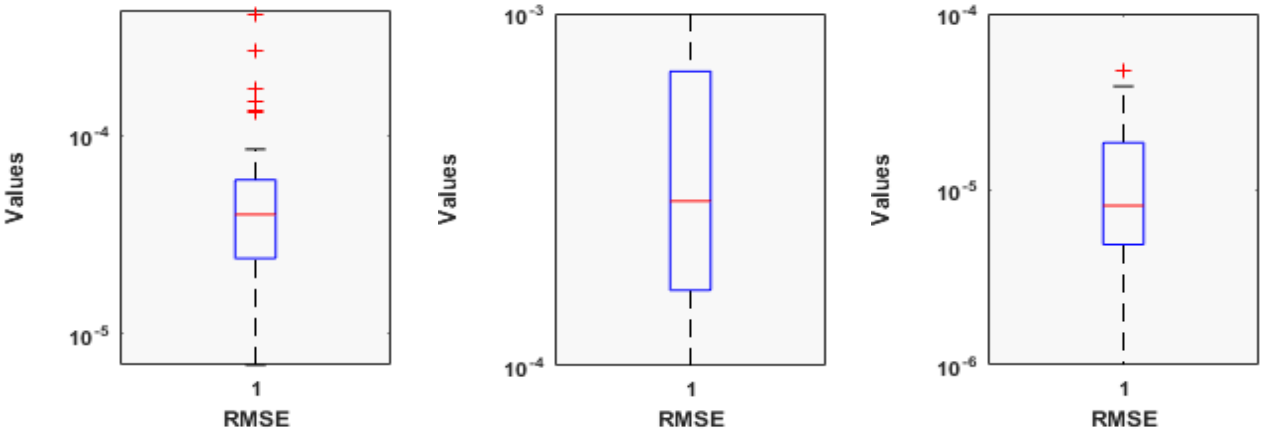

(d) Boxplots: Problem 1. (e) Boxplots: Problem 2. (f) Boxplots: Problem 3.

Figure 5. Convergence investigations of $\hat{V}(\chi)$ for the Problems 1, 2 and 3 MS-TKNS using the Fitness, histograms and boxplots for 10 neurons.

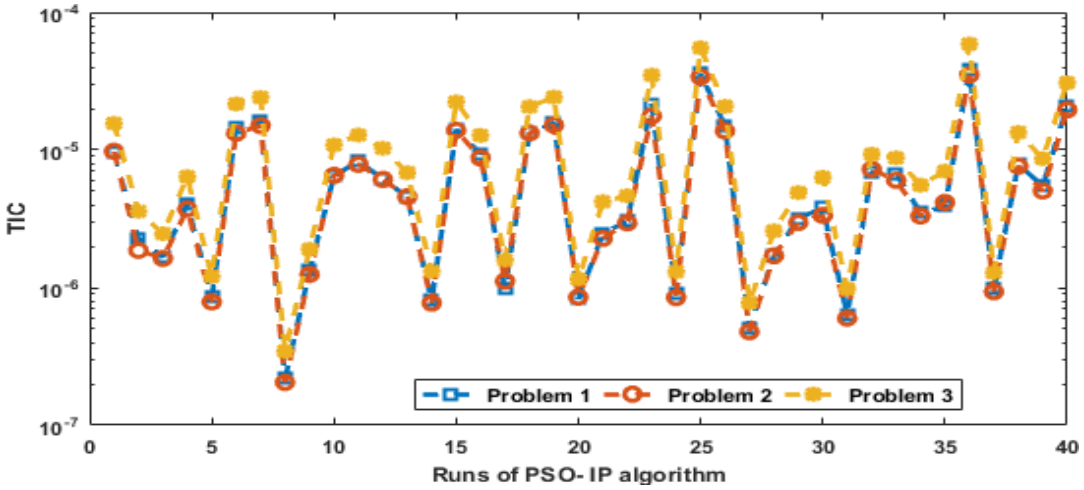

Convergence indices of $\hat{U}(\chi)$ for each problem of the MS-TKNS for the TIC values.

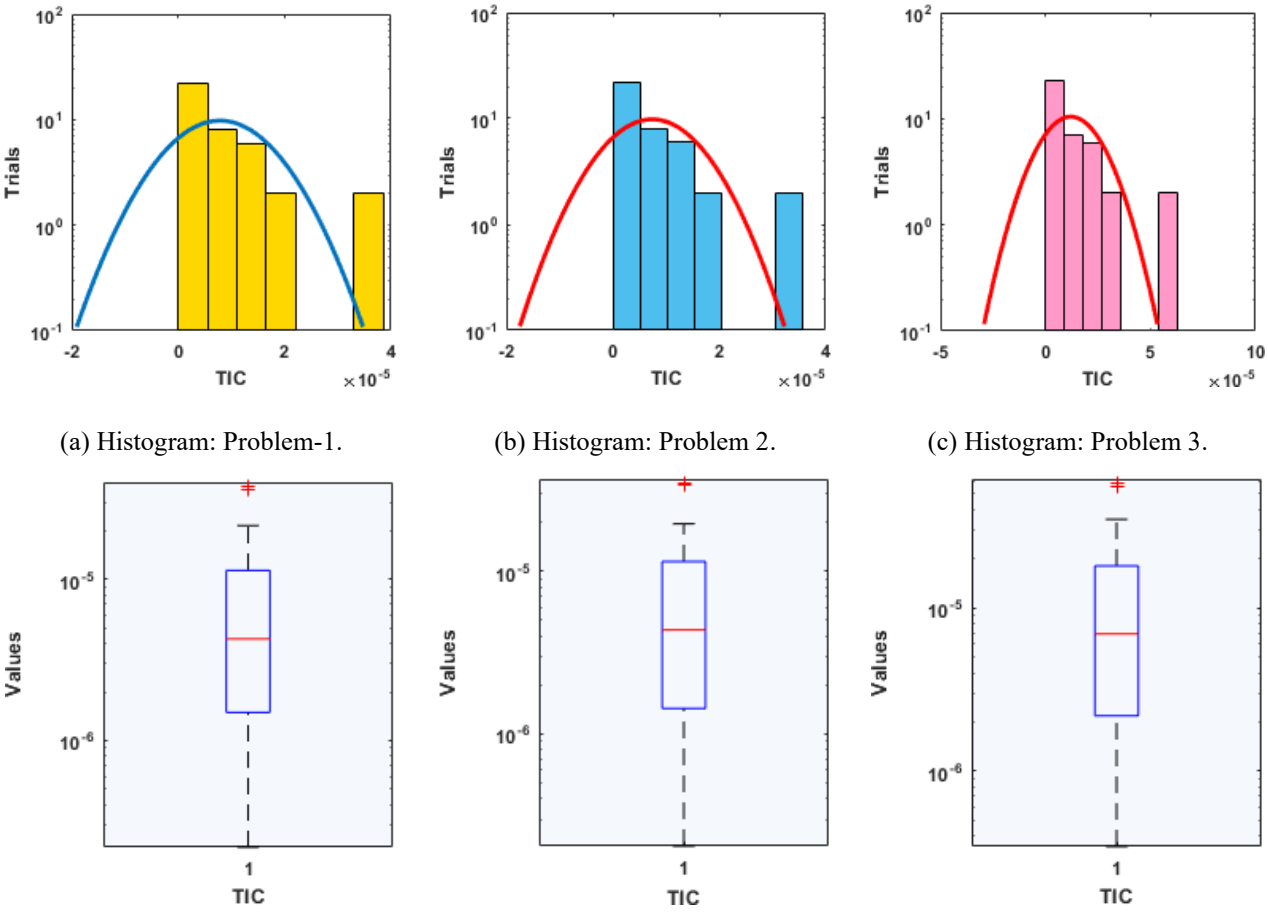

(a) Histogram: Problem-1. (b) Histogram: Problem 2. (c) Histogram: Problem 3.

(d) Boxplots: Problem 1. (e) Boxplots: Problem 2. (f) Boxplots: Problem 3.

Figure 6. Convergence investigations of $\hat{U}(\chi)$ for the Problems 1, 2 and 3 based on the MS-TKNS for the TIC values.

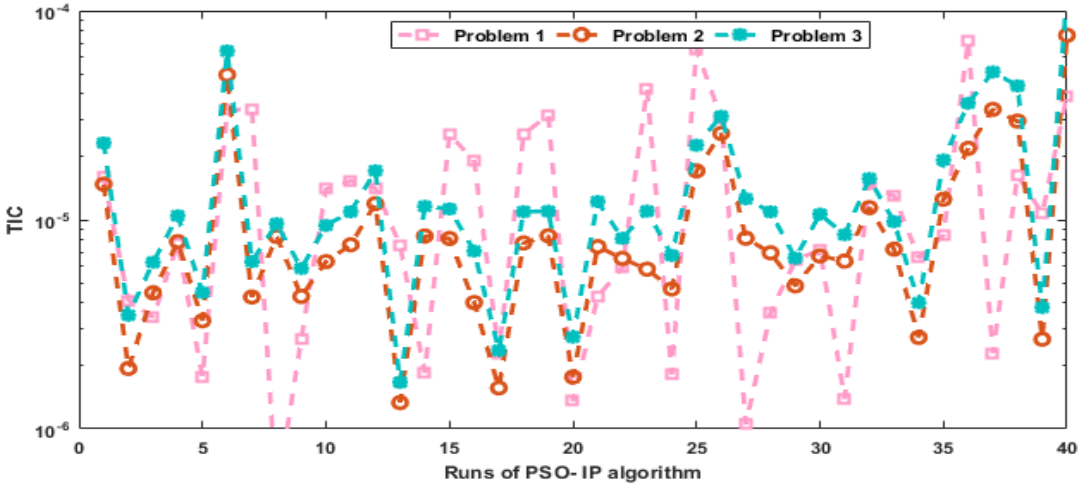

Convergence indices of $\hat{V}(\chi)$ for each problem of the MS-TKNS for the TIC values.

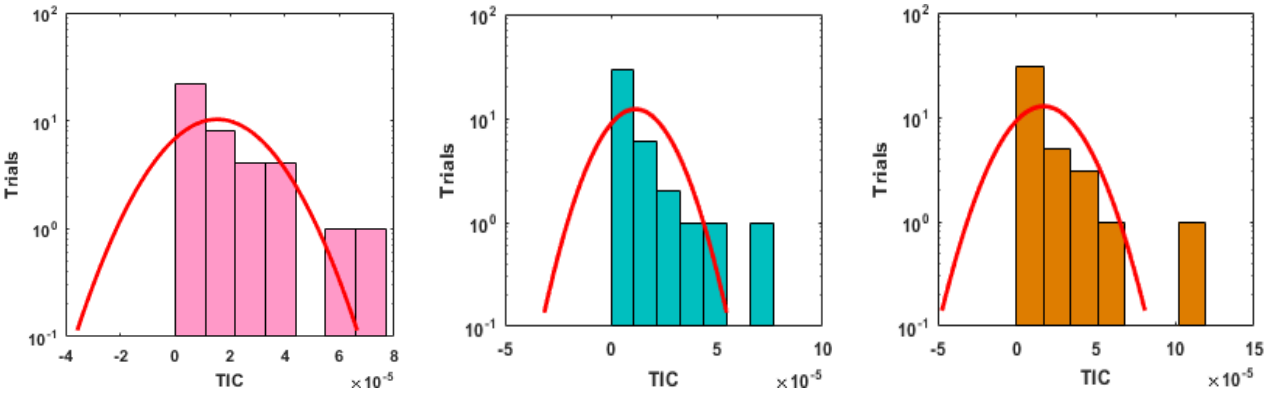

(a) Histogram: Problem-1. (b) Histogram: Problem 2. (c) Histogram: Problem 3.

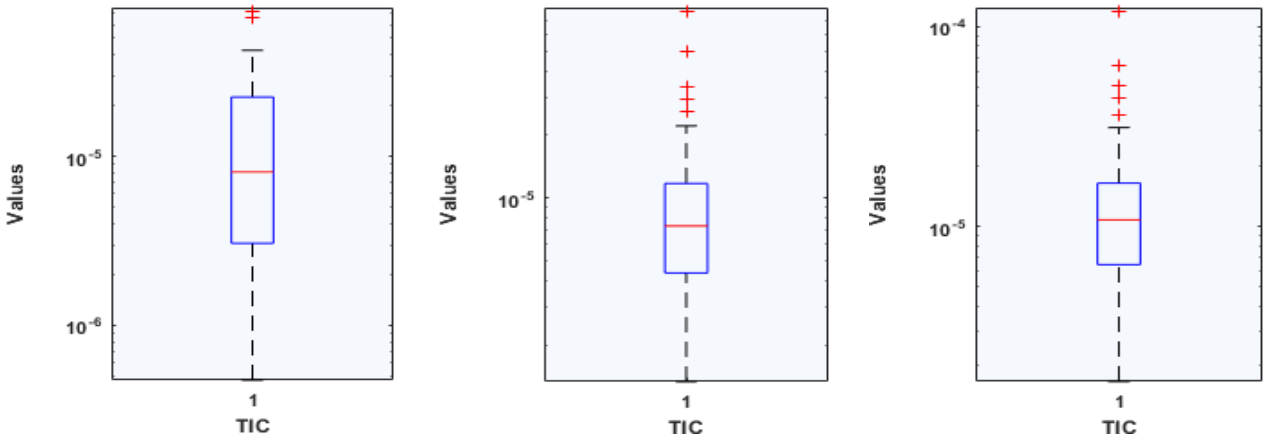

(d) Boxplots: Problem 1. (e) Boxplots: Problem 2. (f) Boxplots: Problem 3.

Figure 7. Convergence investigations of $\hat{V}(\chi)$ for the Problems 1, 2 and 3 based on the MS-TKNS for the TIC values.

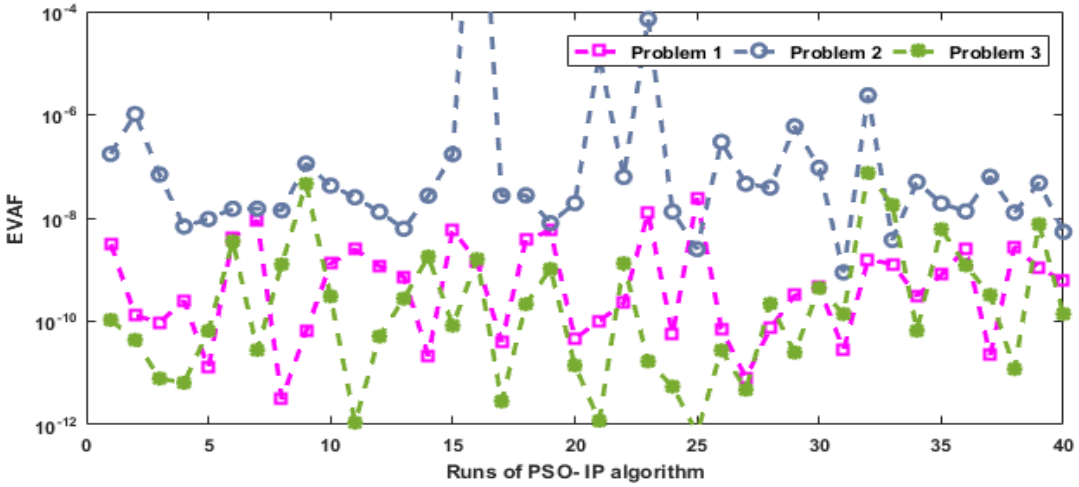

Convergence indices of $\hat{U}(\chi)$ for each problems of the MS-TKNS for the EVAF values.

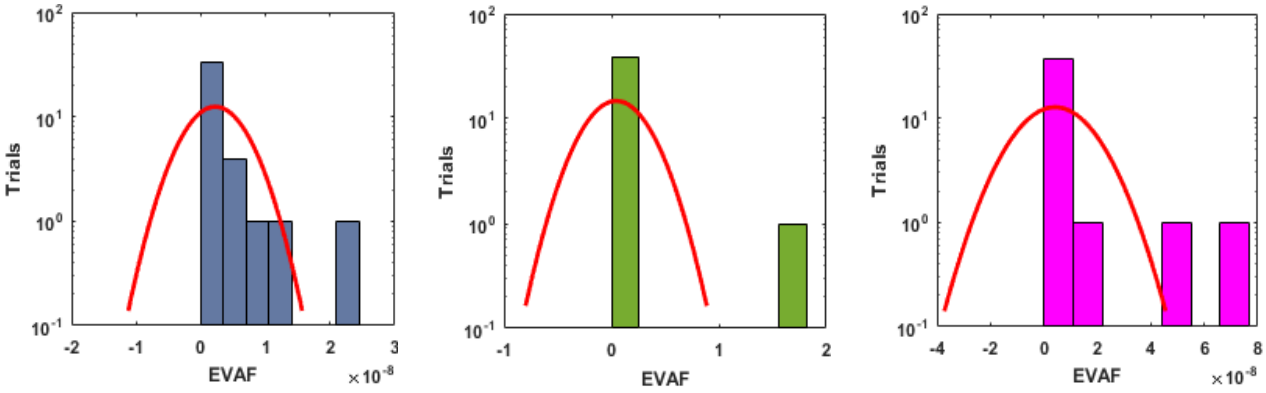

(a) Histogram: Problem-1. (b) Histogram: Problem 2. (c) Histogram: Problem 3.

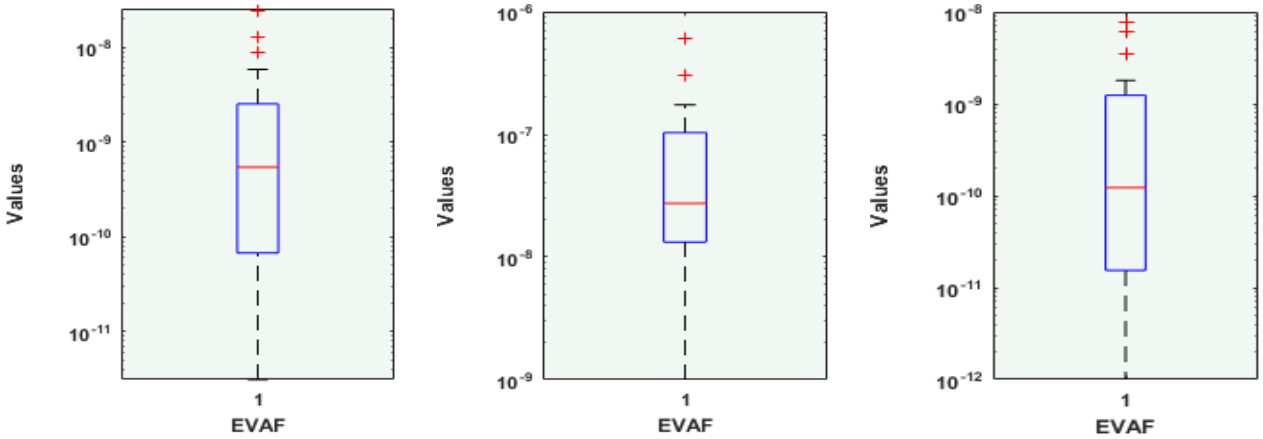

(d) Boxplots: Problem 1. (e) Boxplots: Problem 2. (f) Boxplots: Problem 3.

Figure 8. Convergence measures of $\hat{U}(\chi)$ for the Problems 1, 2 and 3 based on the MS-TKNS using the EVAF values.

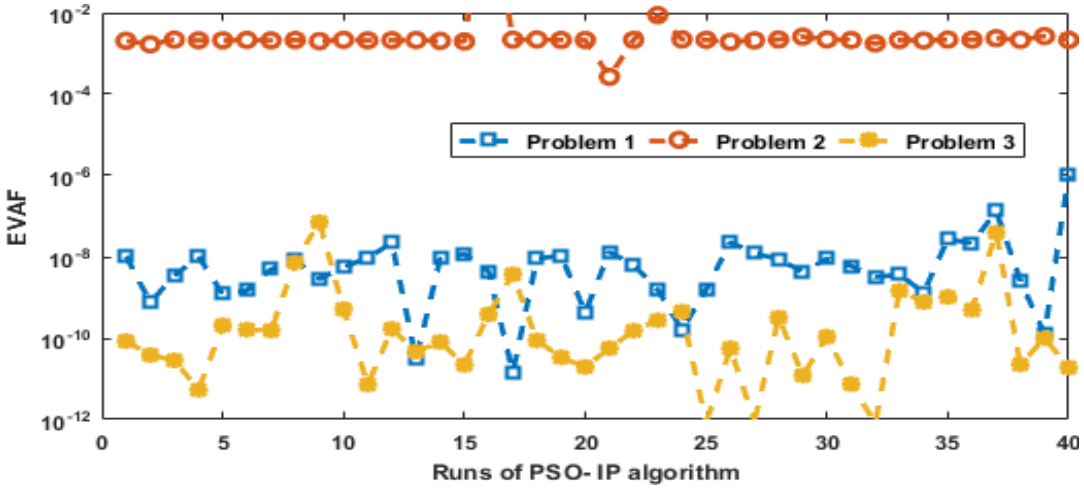

Convergence indices of $\hat{V}(\chi)$ for each problem of the MS-TKNS based on the EVAF

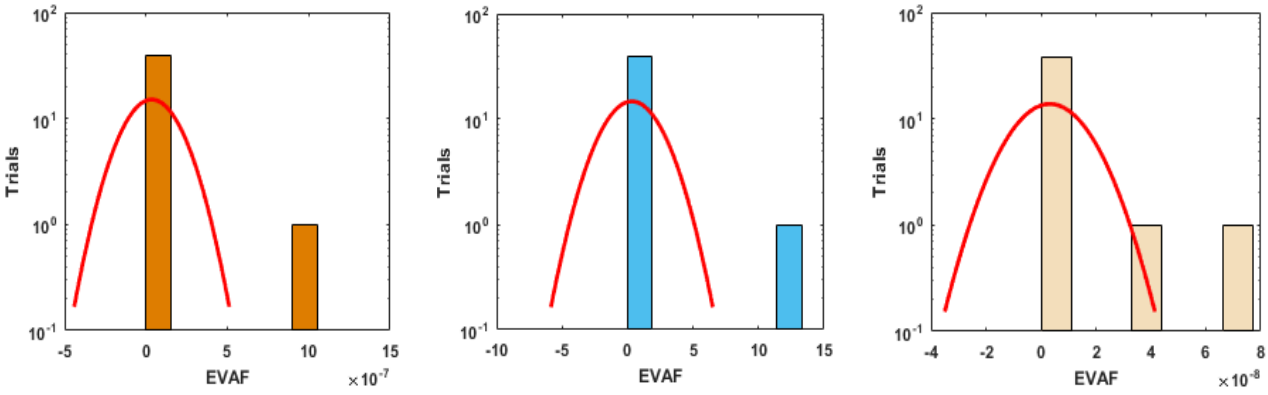

(a) Histogram: Problem-1. (b) Histogram: Problem 2. (c) Histogram: Problem 3.

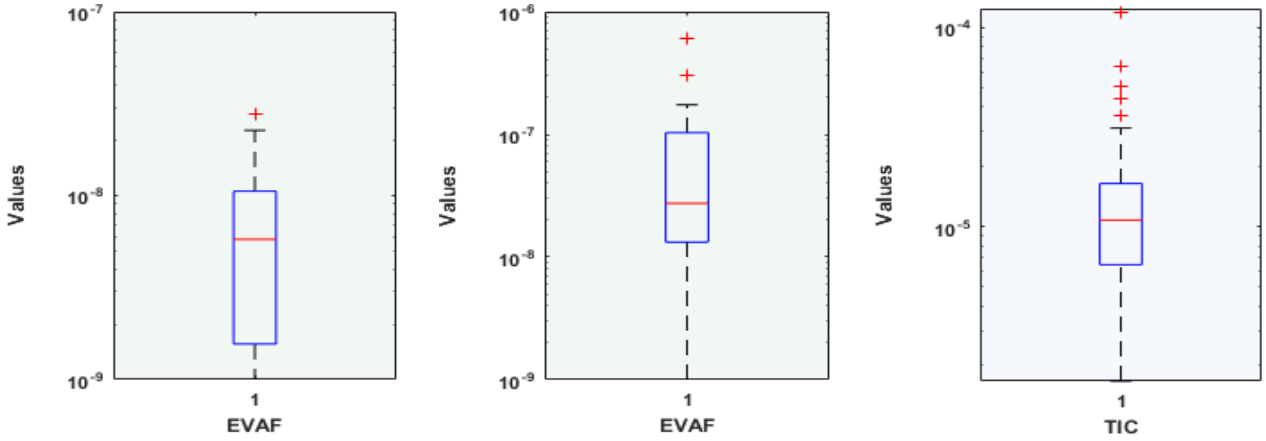

(d) Boxplots: Problem 1. (e) Boxplots: Problem 2. (f) Boxplots: Problem 3.

Figure 9. Convergence measures of $\hat{V}(\chi)$ for the Problems 1, 2 and 3 based on the MS-TKNS for the EVAF, values.

Table 2. The statistics results of $\widehat{U}(\chi)$ for each problem of the MS-TKNS using the designed ANN-PSO-IPA.

	Mode	The solution of $\widehat{U}(\chi)$ for Problems 1–3										
		0	**0.1**	**0.2**	**0.3**	**0.4**	**0.5**	**0.6**	**0.7**	**0.8**	**0.9**	**1**
P-1	Min	3×10^{-7}	1×10^{-7}	6×10^{-7}	7×10^{-7}	5×10^{-7}	1×10^{-7}	8×10^{-7}	8×10^{-7}	4×10^{-7}	1×10^{-7}	5×10^{-7}
	Mean	2×10^{-5}	2×10^{-5}	2×10^{-5}	3×10^{-5}	3×10^{-5}	4×10^{-5}	5×10^{-5}	5×10^{-5}	6×10^{-5}	6×10^{-5}	6×10^{-5}
	SD	4×10^{-5}	4×10^{-5}	4×10^{-5}	4×10^{-5}	4×10^{-5}	5×10^{-5}	5×10^{-5}	6×10^{-5}	6×10^{-5}	6×10^{-5}	6×10^{-5}
	Median	7×10^{-6}	6×10^{-6}	9×10^{-6}	1×10^{-5}	1×10^{-5}	2×10^{-5}	2×10^{-5}	3×10^{-5}	3×10^{-5}	3×10^{-5}	3×10^{-5}
	SIR	1×10^{-5}	1×10^{-5}	1×10^{-5}	1×10^{-5}	2×10^{-5}	3×10^{-5}	3×10^{-5}	3×10^{-5}	3×10^{-5}	3×10^{-5}	4×10^{-5}
P-2	Min	7×10^{-6}	8×10^{-6}	7×10^{-6}	1×10^{-5}	3×10^{-6}	2×10^{-6}	1×10^{-5}	1×10^{-6}	1×10^{-6}	1×10^{-5}	2×10^{-5}
	Mean	3×10^{-3}	3×10^{-3}	3×10^{-3}	3×10^{-3}	4×10^{-3}	6×10^{-3}	1×10^{-2}	1×10^{-2}	2×10^{-2}	4×10^{-2}	5×10^{-2}
	SD	1×10^{-2}	1×10^{-2}	1×10^{-2}	1×10^{-2}	1×10^{-2}	2×10^{-2}	5×10^{-2}	9×10^{-2}	1×10^{-1}	2×10^{-1}	3×10^{-1}
	Median	3×10^{-4}	3×10^{-4}	3×10^{-4}	2×10^{-4}	2×10^{-4}	2×10^{-4}	2×10^{-4}	2×10^{-4}	2×10^{-4}	2×10^{-4}	3×10^{-4}
	SIR	2×10^{-4}	2×10^{-4}	2×10^{-4}	2×10^{-4}	2×10^{-4}	2×10^{-4}	2×10^{-4}	2×10^{-4}	2×10^{-4}	2×10^{-4}	2×10^{-4}
P-3	Min	1×10^{-7}	1×10^{-7}	7×10^{-7}	1×10^{-7}	2×10^{-7}	1×10^{-9}	3×10^{-7}	1×10^{-7}	8×10^{-7}	2×10^{-7}	1×10^{-7}
	Mean	8×10^{-6}	9×10^{-6}	1×10^{-5}	1×10^{-5}	1×10^{-5}	1×10^{-5}	2×10^{-5}	2×10^{-5}	2×10^{-5}	3×10^{-5}	3×10^{-5}
	SD	1×10^{-5}	1×10^{-5}	1×10^{-5}	2×10^{-5}	2×10^{-5}	3×10^{-5}	3×10^{-5}	4×10^{-5}	4×10^{-5}	5×10^{-5}	6×10^{-5}
	Median	3×10^{-6}	3×10^{-6}	3×10^{-6}	5×10^{-6}	6×10^{-6}	7×10^{-6}	8×10^{-6}	1×10^{-5}	1×10^{-5}	1×10^{-5}	1×10^{-5}
	SIR	4×10^{-6}	4×10^{-6}	5×10^{-6}	6×10^{-6}	5×10^{-6}	6×10^{-6}	8×10^{-6}	9×10^{-6}	1×10^{-5}	1×10^{-5}	1×10^{-5}

Table 3. The statistics results of $\hat{v}(\chi)$ for each problem of the MS-TKNS using the designed ANN-PSO-IPA.

	Mode	The solution of $\widehat{U}(\chi)$ for Problems 1–3										
		0	**0.1**	**0.2**	**0.3**	**0.4**	**0.5**	**0.6**	**0.7**	**0.8**	**0.9**	**1**
P-1	Min	7×10^{-7}	4×10^{-7}	1×10^{-7}	1×10^{-6}	1×10^{-7}	1×10^{-6}	8×10^{-7}	2×10^{-6}	8×10^{-7}	3×10^{-6}	5×10^{-6}
	Mean	3×10^{-5}	3×10^{-5}	3×10^{-5}	4×10^{-5}	5×10^{-5}	5×10^{-5}	6×10^{-5}	7×10^{-5}	7×10^{-5}	8×10^{-5}	8×10^{-5}
	SD	5×10^{-5}	4×10^{-5}	5×10^{-5}	5×10^{-5}	6×10^{-5}	7×10^{-5}	8×10^{-5}	9×10^{-5}	9×10^{-5}	1×10^{-4}	1×10^{-4}
	Median	1×10^{-5}	1×10^{-5}	1×10^{-5}	2×10^{-5}	2×10^{-5}	3×10^{-5}	4×10^{-5}	4×10^{-5}	5×10^{-5}	5×10^{-5}	5×10^{-5}
	SIR	1×10^{-5}	1×10^{-5}	1×10^{-5}	1×10^{-5}	1×10^{-5}	2×10^{-5}	2×10^{-5}	2×10^{-5}	2×10^{-5}	2×10^{-5}	2×10^{-5}
P-2	Min	1×10^{-5}	4×10^{-6}	1×10^{-5}	3×10^{-6}	2×10^{-5}	3×10^{-6}	1×10^{-7}	3×10^{-5}	6×10^{-4}	4×10^{-3}	1×10^{-2}
	Mean	1×10^{-3}	5×10^{-3}	1×10^{-2}	2×10^{-2}	3×10^{-2}	4×10^{-2}	4×10^{-2}	5×10^{-2}	5×10^{-2}	6×10^{-2}	9×10^{-2}
	SD	3×10^{-3}	2×10^{-2}	9×10^{-2}	1×10^{-1}	2×10^{-1}	2×10^{-1}	2×10^{-1}	3×10^{-1}	3×10^{-1}	3×10^{-1}	3×10^{-1}
	Median	2×10^{-4}	1×10^{-4}	2×10^{-4}	2×10^{-4}	2×10^{-4}	2×10^{-4}	2×10^{-4}	3×10^{-4}	2×10^{-3}	9×10^{-3}	3×10^{-2}
	SIR	2×10^{-4}	2×10^{-4}	2×10^{-4}	2×10^{-4}	2×10^{-4}	1×10^{-4}	1×10^{-4}	2×10^{-4}	2×10^{-4}	2×10^{-4}	3×10^{-4}
P-3	Min	2×10^{-7}	3×10^{-7}	6×10^{-7}	6×10^{-7}	3×10^{-7}	2×10^{-7}	1×10^{-7}	1×10^{-7}	2×10^{-7}	1×10^{-7}	4×10^{-7}
	Mean	9×10^{-6}	8×10^{-6}	9×10^{-6}	1×10^{-5}	1×10^{-5}	1×10^{-5}	1×10^{-5}	1×10^{-5}	2×10^{-5}	2×10^{-5}	2×10^{-5}
	SD	1×10^{-5}	1×10^{-5}	1×10^{-5}	1×10^{-5}	1×10^{-5}	2×10^{-5}	2×10^{-5}	3×10^{-5}	3×10^{-5}	4×10^{-5}	5×10^{-5}
	Median	3×10^{-6}	2×10^{-6}	3×10^{-6}	4×10^{-6}	5×10^{-6}	6×10^{-6}	8×10^{-6}	8×10^{-6}	9×10^{-6}	1×10^{-5}	1×10^{-5}
	SIR	5×10^{-6}	5×10^{-6}	3×10^{-6}	3×10^{-6}	4×10^{-6}	6×10^{-6}	6×10^{-6}	7×10^{-6}	8×10^{-6}	8×10^{-6}	1×10^{-5}

Table 4. Global performance of $\widehat{U}(\chi)$ and $\widehat{V}(\chi)$ for Problems 1, 2 and 3.

Index	Example	G.FIT		G.RMSE		G.TIC		G.EVAF	
		Mag	Median	Mag	Median	Mag	Median	Mag	Median
$\widehat{U}(\chi)$	1	6×10^{-6}	3×10^{-6}	4×10^{-5}	2×10^{-5}	7×10^{-6}	4×10^{-6}	2×10^{-9}	5×10^{-10}
	2	2×10^{-4}	4×10^{-5}	2×10^{-2}	2×10^{-4}	7×10^{-6}	4×10^{-6}	4×10^{-2}	2×10^{-7}
	3	1×10^{-6}	3×10^{-7}	2×10^{-5}	9×10^{-6}	1×10^{-5}	6×10^{-6}	4×10^{-9}	1×10^{-10}
$\widehat{V}(\chi)$	1	6×10^{-6}	3×10^{-6}	6×10^{-5}	4×10^{-5}	1×10^{-5}	8×10^{-6}	3×10^{-7}	5×10^{-9}
	2	2×10^{-4}	4×10^{-5}	5×10^{-2}	1×10^{-2}	1×10^{-5}	7×10^{-6}	3×10^{-1}	2×10^{-3}
	3	1×10^{-6}	3×10^{-7}	1×10^{-5}	8×10^{-6}	1×10^{-5}	1×10^{-5}	3×10^{-9}	9×10^{-11}

5. Conclusions

In this research study, a stable, reliable and accurate numerical ANN-PSO-IPA is accessible to solve the multi-singular nonlinear third kind of Emden-Fowler system by using the ANN strength with continuous mapping. A fitness function of these networks is optimized for the global and local search capabilities of particle swarm optimization and interior-point algorithm, respectively. The proposed ANN-PSO-IPA is broadly applied to solve three different variants of the multi-singular nonlinear third kind of Emden-Fowler system. The precise and accurate performance is observed for ANN-PSO-IPA based on AE with consistent precision around 5 to 8 decimal places of precision for all three problems of the multi-singular nonlinear third kind of Emden-Fowler system. Statistical interpretations in terms of Min, Mean, SD, SI ranges and Median are performed to validate the convergence, robustness and accuracy of the proposed ANN-PSO-IPA for solving the multi-singular nonlinear third kind of Emden-Fowler system based Eqs 1–3.

In the future, new stochastic solvers based on ANN optimized with evolutionary/swarming paradigm looks proficient to solve nonlinear biological systems [47–50], fluid dynamics models [51–56] and fractional models [57–60]. Additionally, the different ANNs structure exploiting variety of activation functions should be implemented to solve the MS-TKNS for improved performance.

Acknowledgments

This paper has been partially supported by Ministerio de Ciencia, Innovacion y Universidades grant number PGC2018-0971-B-100 and Fundacion Seneca de la Region de Murcia grant number 20783/PI/18.

Conflict of interest

All the authors of the manuscript declared that there are no potential conflicts of interest.

References

1. H. J. Lane, On the Theoretical Temperature of the Sun, under the Hypothesis of a gaseous Mass maintaining its Volume by its internal Heat and depending on the laws of gases as known to terrestrial Experiment, *Am. J. Sci.*, **148** (1870), 57–74.
2. R. Emden, *Gaskugeln Teubner*, Leipzig und Berlin, 1907.

3. I. Ahmad, M. A. Z. Raja, M. Bilal, F. Ashraf, Neural network methods to solve the Lane–Emden type equations arising in thermodynamic studies of the spherical gas cloud model, *Neural Comput. Appli.*, **28** (2017), 929–944.
4. T. C. Hao, F. Z. Cong, Y. F. Shang, An efficient method for solving coupled Lane–Emden boundary value problems in catalytic diffusion reactions and error estimate, *J. Math. Chem.*, **56** (2018), 2691–2706.
5. T. Luo, Z. Xin, H. Zeng, Nonlinear asymptotic stability of the Lane-Emden solutions for the viscous gaseous star problem with degenerate density dependent viscosities, *Commun. Math. Phys.*, **347** (2016), 657–702.
6. F. Abbas, P. Kitanov, S. Longo, Approximate solutions to lane-emden equation for stellar configuration, *Appl. Math. Inf. Sci.*, **13** (2019), 143–152.
7. M. A. Soliman, Approximate solution for the Lane-Emden equation of the second kind in a spherical annulus, *J. King Saud Univ., Eng. Sci.*, **31** (2019), 1–5.
8. V. Radulescu, D. Repovs, Combined effects in nonlinear problems arising in the study of anisotropic continuous media, *Nonlinear Anal.: Theory, Methods Appl.*, **75** (2012), 1524–1530.
9. J. A. Khan, M. A. Z. Raja, M. M. Rashidi, M. I. Syam, A. M. Wazwaz, Nature-inspired computing approach for solving non-linear singular Emden–Fowler problem arising in electromagnetic theory, *Connect. Science*, **27** (2015), 377–396.
10. M. Ghergu, V. Radulescu, On a class of singular Gierer–Meinhardt systems arising in morphogenesis, *C. R. Math.*, **344** (2007), 163–168.
11. A. K. Dizicheh, S. Salahshour, A. Ahmadian, D. Baleanu, A novel algorithm based on the Legendre wavelets spectral technique for solving the Lane–Emden equations, *Appl. Numer. Math.*, **153** (2020), 443–456.
12. W. Adel, Z. Sabir, Solving a new design of nonlinear second-order Lane–Emden pantograph delay differential model via Bernoulli collocation method, *Eur. Phys. J. Plus*, **135** (2020), 427.
13. Z. Sabir, M. G. Sakar, M. Yeskindirova, O. Saldir, Numerical investigations to design a novel model based on the fifth order system of Emden–Fowler equations, *Theor. Appl. Mech. Lett.*, **10** (2020), 333–342.
14. R. Singh, V. Guleria, M. Singh, Haar wavelet quasilinearization method for numerical solution of Emden–Fowler type equations, *Math. Comput. Simul.*, **174** (2020), 123–133.
15. M. A. Abdelkawy, Z. Sabir, J. L. Guirao, T. Saeed, Numerical investigations of a new singular second-order nonlinear coupled functional Lane–Emden model, *Open Phys.*, **18** (2020), 770–778.
16. Z. Sabir, H. Günerhan, J. L. Guirao, On a new model based on third-order nonlinear multisingular functional differential equations, *Math. Probl. Eng.*, **2020** (2020), 1–9.
17. A. M. Wazwaz, A new algorithm for solving differential equations of Lane–Emden type, *Appl. Math. Comput.*, **118** (2001), 287–310.
18. Z. Sabir, H. A. Wahab, M. Umar, M. G. Sakar, M. A. Z. Raja, Novel design of Morlet wavelet neural network for solving second order Lane–Emden equation, *Math. Comput. Simul.*, **172** (2020), 1–14.
19. A. H. Bukhari, M. Sulaiman, S. Islam, M. Shoaib, P. Kumam, M. A. Z. Raja, Neuro-fuzzy modeling and prediction of summer precipitation with application to different meteorological stations, *Alexandria Eng. J.*, **59** (2020), 101–116.

20. Z. Sabir, M. A. Z. Raja, J. L. Guirao, M. Shoaib, A novel design of fractional Meyer wavelet neural networks with application to the nonlinear singular fractional Lane-Emden systems. *Alexandria Eng. J.*, **60** (2021), 2641–2659.
21. M. A. Z. Raja, M. Umar, Z. Sabir, J. A. Khan, D. Baleanu, A new stochastic computing paradigm for the dynamics of nonlinear singular heat conduction model of the human head, *Eur. Phys. J. Plus*, **133** (2018), 1–21.
22. M. A. Z. Raja, Z. Sabir, N. Mehmood, E. S. Al-Aidarous, J. A. Khan, Design of stochastic solvers based on genetic algorithms for solving nonlinear equations, *Neural Comput. Appl.*, **26** (2015), 1–23.
23. A. H. Bukhari, M. A. Z. Raja, M. Sulaiman, S. Islam, M. Shoaib, P. Kumam, Fractional neuro-sequential ARFIMA-LSTM for financial market forecasting, *IEEE Access*, **8** (2020), 71326–71338.
24. M. Umar, Z. Sabir, M. A. Z. Raja, Intelligent computing for numerical treatment of nonlinear prey–predator models, *Appl. Soft Comput.*, **80** (2019), 506–524.
25. Z. Sabir, H. A. Wahab, M. Umar, F. Erdoğan, Stochastic numerical approach for solving second order nonlinear singular functional differential equation, *Appl. Math. Comput.*, **363** (2019), 124605.
26. Z. Sabir, M. A. Z. Raja, M. Umar, M. Shoaib, Neuro-swarm intelligent computing to solve the second-order singular functional differential model, *Eur. Phys. J. Plus*, **135** (2020), 1–19.
27. M. Umar, Z. Sabir, M. A. Z. Raja, F. Amin, T. Saeed, Y. Guerrero-Sanchez, Integrated neuro-swarm heuristic with interior-point for nonlinear SITR model for dynamics of novel COVID-19, *Alexandria Eng. J.*, **60** (2021), 2811–2824.
28. M. Umar, Z. Sabir, M. A. Z. Raja, M. Shoaib, M. Gupta, Y. G. Sánchez, A Stochastic Intelligent Computing with Neuro-Evolution Heuristics for Nonlinear SITR System of Novel COVID-19 Dynamics, *Symmetry*, **12** (2020), 1628.
29. J. L. Guirao, Z. Sabir, T. Saeed, Design and numerical solutions of a novel third-order nonlinear Emden–Fowler delay differential model, *Math. Probl. Eng.*, **2020** (2020), 1–9.
30. Z. Sabir, M. A. Z. Raja, J. L. Guirao, M. Shoaib, A Neuro-Swarming Intelligence-Based Computing for Second Order Singular Periodic Non-linear Boundary Value Problems, *Front. Phys.*, **8** (2020), 224.
31. M. Umar, Z. Sabir, F. Amin, J. L. Guirao, M. A. Z. Raja, Stochastic numerical technique for solving HIV infection model of CD4+ T cells, *Eur. Phys. J. Plus*, **135** (2020), 403.
32. M. Umar, Z. Sabir, M. A. Z. Raja, Y. G. Sánchez, A stochastic numerical computing heuristic of SIR nonlinear model based on dengue fever, *Results Phys.*, **19** (2020), 103585.
33. T. T. Teo, T. Logenthiran, W. L. Woo, K. Abidi, T. John, N. S. Wade, et al., Optimization of Fuzzy Energy-Management System for Grid-Connected Microgrid Using NSGA-II, *IEEE Trans. Cybern.*, **2020** (2020), 1–12.
34. C. S. Chin, X. Ji, W. L. Woo, T. J. Kwee, W. Yang, Modified multiple generalized regression neural network models using fuzzy C-means with principal component analysis for noise prediction of offshore platform, *Neural Comput. Appl.*, **31** (2019), 1127–1142.
35. A. M. Wazwaz, The variational iteration method for solving systems of third-order Emden-Fowler type equations, *J. Math. Chem.*, **55** (2017), 799–817.
36. T. V. Sibalija, Particle swarm optimisation in designing parameters of manufacturing processes: A review (2008–2018), *Appl. Soft Comput.*, **84** (2019), 105743.

37. A. P. Engelbrecht, Particle swarm optimization with crossover: a review and empirical analysis, *Artif. Intell. Rev.*, **45** (2016), 131–165.
38. A. Mehmood, A. Zameer, M. A. Z. Raja, R. Bibi, N. I. Chaudhary, M. S. Aslam, Nature-inspired heuristic paradigms for parameter estimation of control autoregressive moving average systems, *Neural Comput. Appl.*, **31** (2019), 5819–5842.
39. A. Mehmood, A. Zameer, M. S. Aslam, M. A. Z. Raja, Design of nature-inspired heuristic paradigm for systems in nonlinear electrical circuits, *Neural Compu. Appl.*, **32** (2020), 7121–7137.
40. D. Bouhadjra, A. Kheldoun, A. Zemouche, Performance analysis of stand-alone six-phase induction generator using heuristic algorithms, *Math. Comput. Simul.*, **167** (2020), 231–249.
41. H. Mesloub, M. T. Benchouia, R. Boumaaraf, A. Goléa, N. Goléa, M. Becherif, Design and implementation of DTC based on AFLC and PSO of a PMSM, *Math. Comput. Simul.*, **167** (2020), 340–355.
42. M. A. Z. Raja, A. Zameer, A. K. Kiani, A. Shehzad, M. A. R. Khan, Nature-inspired computational intelligence integration with Nelder–Mead method to solve nonlinear benchmark model, *Neural Compu. Appl.*, **29** (2018), 1169-1193.
43. L. Casacio, C. Lyra, A. R. Oliveira, Interior point methods for power flow optimization with security constraints, *Int. Trans. Oper. Res.*, **26** (2019), 364–378.
44. A. Zanelli, A. Domahidi, J. Jerez, M. Morari, FORCES NLP: an efficient implementation of interior-point methods for multistage nonlinear nonconvex programs, *Int. J. Control*, **93** (2020), 13–29.
45. E. Chouzenoux, M. C. Corbineau, J. C. Pesquet, A proximal interior point algorithm with applications to image processing, *J.Math. Imaging Vision*, **2019** (2019), 1–22.
46. Z. Sabir, M. A. Zahoor Raja, D. Baleanu, Fractional Mayer Neuro-swarm heuristic solver for multi-fractional Order doubly singular model based on Lane-Emden equation, *Fractals*, **29** (2021), 2140017.
47. W. Gao, G. Yel, H. M. Baskonus, C. Cattani, Complex solitons in the conformable (2+1)-dimensional Ablowitz-Kaup-Newell-Segur equation, *Aims Math.*, **5** (2020), 507–521.
48. H. M. Baskonus, H. Bulut, T. A. Sulaiman, New complex hyperbolic structures to the lonngren-wave equation by using sine-gordon expansion method, *Appl. Math. Nonlinear Sci.*, **4** (2019), 129–138.
49. Y. G. Sanchez, Z. Sabir, J. L. Guirao, Design of a nonlinear SITR fractal model based on the dynamics of a novel coronavirus (COVID), *Fractals*, **28** (2020), 2040026.
50. T. N. Cheema, M. A. Z. Raja, I. Ahmad, S. Naz, H. Ilyas, M. Shoaib, Intelligent computing with Levenberg–Marquardt artificial neural networks for nonlinear system of COVID-19 epidemic model for future generation disease control, *Eur. Phys. J. Plus*, **135** (2020), 1–35.
51. M. Umar, Z. Sabir, A. Imran, A. H. Wahab, M. Shoaib, M. A. Z. Raja, The 3-D flow of Casson nanofluid over a stretched sheet with chemical reactions, velocity slip, thermal radiation and Brownian motion, *Therm. Sci.*, **24** (2020), 2929–2939.
52. I. Uddin, I. Ullah, M. A. Z. Raja, M. Shoaib, S. Islam, T. Muhammad, Design of intelligent computing networks for numerical treatment of thin film flow of Maxwell nanofluid over a stretched and rotating surface, *Surf. Interfaces*, **24** (2021), 101107.
53. J. L. Aljohani, E. S. Alaidarous, M. A. Z. Raja, M. Shoaib, M. S. Alhothuali, Intelligent computing through neural networks for numerical treatment of non-Newtonian wire coating analysis model, *Sci. Rep.*, **11** (2021), 1–32.

54. M. Dewasurendra, K. Vajravelu, On the method of inverse mapping for solutions of coupled systems of nonlinear differential equations arising in nanofluid flow, heat and mass transfer, *Appl. Math. Nonlinear Sci.*, **3** (2018), 1–14.
55. P. Lakshminarayana, K. Vajravelu, G. Sucharitha, S. Sreenadh, Peristaltic slip flow of a Bingham fluid in an inclined porous conduit with Joule heating, *Appl. Math. Nonlinear Sci.*, **3** (2018), 41–54.
56. Z. Sabir, M. G. Sakar, M. Yeskindirova, O. Saldir, Numerical investigations to design a novel model based on the fifth order system of Emden–Fowler equations, *Theor. Appl. Mech. Lett.*, **10** (2020), 333–342.
57. E. İlhan, İ. O. Kıymaz, A generalization of truncated M-fractional derivative and applications to fractional differential equations, *Appl. Math. Nonlinear Sci.*, **5** (2020), 171–188.
58. D. W. Brzeziński, Review of numerical methods for NumILPT with computational accuracy assessment for fractional calculus, *Appl. Math. Nonlinear Sci.*, **3** (2018), 487–502.
59. E. İlhan, İ. O. Kıymaz, A generalization of truncated M-fractional derivative and applications to fractional differential equations, *Appl. Math. Nonlinear Sci.*, **5** (2020), 171–188.
60. D. W. Brzeziński, Comparison of fractional order derivatives computational accuracy-right hand vs left hand definition, *Appl. Math. Nonlinear Sci.*, **2** (2017), 237–248.

AIMS Press